Supplementary Information

Stonehenge's geometry and counts recover interior dimensions and select Cygnus near 3000 BCE

Lucas Giovani Ribeiro and Marcos André Simonssini

This document collects extended results, mathematical derivations and comparison tables. Main Methods supplies the operational definitions. Supplementary Data 1 contains the executable research record, the original S1 and S5 notes, and complete numerical outputs. Construction_Sequence reproduces the current Figure 2 and its derived interior consistency check. Figure6_Sky_Comparison reproduces the new main Figure 6; S11 retains the full-window comparison.

Reading order

S9 — Archaeological inputs, dimensional and directional results, regional comparisons and source controls. S9.9 adds operation comparisons and measurement decision bounds.

S6 — Geometric role recovery, median certificates and persistence.

S7 — Regional scale-free and horizon comparisons.

S8 — Complete circular-field census, calibration, invariance and common-epoch dominance.

S10 — Four-position extension, conditional inverse, midpoint ablations, material-rule census and procedure diagnostic.

S11 — Woodhenge ring inputs, chronological concordance, arithmetic target census, random-inventory comparisons, material transcription and conditional recovery.

Numbering and reproducibility

The S-labels preserve links to the archived data and scripts. References use the current main bibliography. The addition of Marshall et al. as reference 33 shifts the former references 33–44 to 34–45; citations in the current reading components have been reconciled. Historical documents retain their original numbering, with crosswalks supplied. S6–S10 scientific content is preserved; S11 includes the Woodhenge analysis and the v1.51 random-inventory comparisons.

Principal comparisons

Exterior-only recovery: 2.02% RMS; first among 212,520 assignments in the 23-operation comparison. S9.9 tests an expanded library and gives measurement sensitivity bounds. Fixed-scale field census: Cygnus first among 19,939 fields near 2965 BCE, runner-up error ratio 2.2013. Woodhenge: among 5,832 arithmetic targets, 33 global optima fall in the construction interval and one also has RMS below 0.2°, near 2609 BCE. Calibration, midpoint, alternative-epoch and positional controls remain in their respective sections.

Extended architectural and selection analyses

Supplementary Material S9

Operational definitions are given in main Methods. This section reports the associated results and derivations; executable instructions and the complete historical records are in Supplementary Data 1.

Lucas Giovani Ribeiro and Marcos André Simonssini
Supplementary Information | Stonehenge v1.50 | 30 October 2026

This supplement provides source definitions, algebraic derivations, constructive tests, regional comparisons and phase controls supporting the main results. Citations use the main bibliography. Supplementary Notes belong to S1, while S5–S8 retain their own section numbering. All comparisons are retrospective; their candidate families and retained assumptions are specified at the point of use. Section S9.8 records information order, execution scope and the numbering crosswalk.

S9.1 Sources, measurements and drawing proxies

The primary objects are the Aubrey circuit, the four Station positions, the Sarsen outer envelope, the transverse Trilithon-horseshoe span and the Y- and Z-hole circuits. The Sarsen outer envelope is distinguished from the published inner-face diameter [26]. The four inventory counts are A=56 Aubrey positions, B=30 outer sarsen uprights, C=10 trilithon uprights and D=4 Station positions. These refer to the reconstructed inventory across the monument's history, including absent settings; the four counts do not describe an inventory present at one date. Table S9.1 defines the notation and distinguishes the evidential status of the inputs.

Table S9.1. Operational notation and evidential status. Published measurements, approximate summaries, digitized proxies and model assumptions enter different operations; their sources and boundaries are specified in S9.1–S9.2 and S9.5. The reconstructed inventory spans construction phases.

Symbol or input	Meaning and use	Evidential status
N, s	Aubrey and Station outer counts; N=A and s=D	Published archaeological reconstruction; includes absent settings.
a, b, c	Primitive short leg, long leg and hypotenuse	Derived frame selected within the declared comparison class.
A, B, C, D	Aubrey, sarsen, trilithon and Station inventory	Reconstructed counts across phases, not a simultaneous surviving inventory.
r, g, j, v	Radial, axial, longitudinal and latitudinal seeds	Derived outputs of the specified count map.
Q	Ordered eight-value register	Deterministic expansion of the seeds.

Symbol or input	Meaning and use	Evidential status
W	Ordered temporal triple	Derived numerical target; its timing interpretation is stipulated.
u	Common terrestrial scale	Parameter fitted only to the declared exterior dimensions.
Exterior measures	Published Station sides and Aubrey diameter	Published measurements with stated feature boundaries and source conventions.
Interior measures	Trilithon span, Sarsen outer envelope, Y/Z diameters	Rounded plan readings and approximate published circuit diameters; excluded from scale fitting.
Plan coordinates	Cleal symbols and Rees labels or hatch centroids	Digitized drawing proxies; no measured per-feature survey uncertainty.
Roles and timing scale	Outer 10:24:26; inner 4,10,12,16; minute-per-numerical-unit convention	Declared model choices. The geometric roles were recognized with the plan available.
Perturbation bounds	Side factors, interior ±20% factors and ±0.25 m coordinate scenarios	Stipulated sensitivity distributions or bounds, not measured archaeological errors.

The published Station centre-to-centre distances are 34.17 and 32.70 m for the short sides and 79.93 and 80.26 m for the long sides [23,24]. Stations 91 and 93 survive; 92 and 94 are archaeologically located absent-stone settings. The primary Aubrey diameter is the 86.44 m Thom survey value tabulated by MacKie [24]. Alternative published conventions span 85.832–87.0 m [24,25]. The approximately 13.7 m trilithon span and 33.0 m sarsen outer envelope are rounded readings from Cleal Plan 1; the 39.0 m Z-hole and 54.0 m Y-hole circuit diameters are approximate published summaries [1, p. 260]. Hole diameters pass through hole centres; the Sarsen measure concerns its occupied outer envelope. The inner-face convention [26] is retained as a sensitivity. The ditch [27] and Heel Stone are excluded from calibration and the inner ladder. Supplementary Note 2 records boundaries, sources and precision classes.

We examine two specifications of the route choice. A joint enumeration applies the 34/62 nearest-integer length labels and orthogonal output axes to four symmetric route classes (Supplementary Note 54). An alternative entrance-based selector chooses between the two contour families by alignment with the entrance normal and between the two crossed families by alignment with its perpendicular. It then inspects mean lengths across each selected pair of mirrored routes; the inner-opening normals do not enter this selector (Supplementary Note 40).

S9.2 Count map, inverse and stellar register

Alongside its measured lengths, the monument supplies four architectural counts. These counts generate the ordered seeds through one map:

r=A−B−C=16; g=C=10; j=B+D=34; v=A+C−D=62.

With q=24 and d=28, their expansion is:

Q=(r,q,d,j,d+q,v,3q,v+j)=(16,24,28,34,52,62,72,96).

The inverse recovers the four counts from the ordered seeds:

A=(r+j+v)/2; B=(−r−2g+j+v)/2; C=g; D=(r+2g+j−v)/2.

Exchanging j=34 and v=62 changes the recovered Station count from four to 32. The unchanged inverse returns (56,30,10,4) in the specified order and (56,30,10,32) under exchange, leaving the other three counts unchanged (main Figure 3a). The ordered stellar roles therefore have an explicit consequence within the reconstruction.

The three specified closures admit exactly one strictly positive integer inventory within the fixed compiler, with no upper bound imposed on inventory size: (56,30,10,4). The conditions are $r=D^2$, $d=A/2$ and $p^2=g^2+q^2$, where $p=A-B$. The same solution supplies the doubled frame (g,q,p)=(10,24,26) and W=(28,72,16). Within these conditions, both the inventory and its overall size are fixed. The factorization proof and condition-removal controls are in Supplementary Note 29; the frame and word follow from this conditional solution (main Figure 3b).

The relation can also be read directly from the outer counts and primitive frame. With N=56, s=4 and (a,b,c)=(5,12,13), the identities $N=2s(b-a)$ and $N+s^2=s(c+a)$ give $W=s(b-a,c+a,s)=(N/2,N+s^2,s^2)$. The outer inventories yield 56−30=26 and 30−26=4. These equivalent expressions locate the same frame and word in the chosen material system; their full algebraic and quadratic Gram forms are preserved in Supplementary Notes 17–19 and 52.

Two of 40,960,000 ordered maps return the target seeds, and both are invertible. The comparison is complete and bounded, with each coefficient restricted to −1, 0 or 1. A separate enumeration over ordered count quadruples with entries from 1 to 60 finds that 2.55% can express all four targets within this coefficient class. These are conditional counts of formula and input flexibility; the classes and wider-coefficient sensitivity are specified in Supplementary Notes 5 and 11.

The primary J2000 stellar descriptors are g=10.488°, j=34.078° and v=62.160°, rounding to (10,34,62). Propagating stellar positions to 2965.2 BCE while retaining the fixed J2000 ecliptic frame gives (10.485°,34.075°,62.141°), with the same rounded tuple. With material r=16, these descriptors supply the same Q and inverse. Fixed-plane stability is retained across the declared 10,000-year window under both archived motion prescriptions (Supplementary Notes 24 and 33).

A second, explicitly conditioned route uses contrasts. Given D=4, q=24 and d=28, the compiler gives A=q+d+D=56 and B−C=q−D=20. Adding $r=D^2=16$ gives B+C=40, hence B=30 and C=10. This recovers the inventory for both tested absolute tuples, (10,34,62) and (11,35,63). Without rounding the ancient contrasts, the same inventory uniquely minimizes the constrained squared error: RMS 0.128°, compared with 0.686° for the next inventory (Supplementary Notes 28 and 33).

Historical catalogues provide a further portability comparison. Their Cygnus figures retain an approximately 16° minimum-cover radial scale; the Ulugh Beg values also round to (10,34,62), whereas Ptolemy's values produce a non-target inverse [28]. The detailed catalogue readings, modern coordinate definitions and provenance of the prior grammar are preserved together in Supplementary Table S53.1 and Notes 7–8. Here the radial seed remains a material input.

S9.3 Dimensional recovery and phase structure

The 5:12:13 rectangle ranks first among the 16 primitive candidates, with 1.57% side RMS against 6.64% for the next candidate, 36:77:85. Combining metric and cyclic comparisons again selects 5:12:13 with the 7|21|7|21 partition, first among 208 combinations. It remains first in every side-perturbation trial at ±1% and ±2%; at ±5%, it remains first in 96.72% of metric-only and 97.63% of joint trials. Main Figure 1 locates the archaeological setting and the exterior positions used by the reconstruction.

The discrete construction gives hypotenuse-normalized legs 4.975 and 12.010, with 0.36% RMS against 5 and 12. At the independently published 86.44 m diameter, its chords are 33.08 and 79.86 m, differing from the observed short- and long-side means by −1.06% and −0.29%. The side ratio therefore supports 7|21|7|21 as an approximate discrete shape (Figure S9.1).

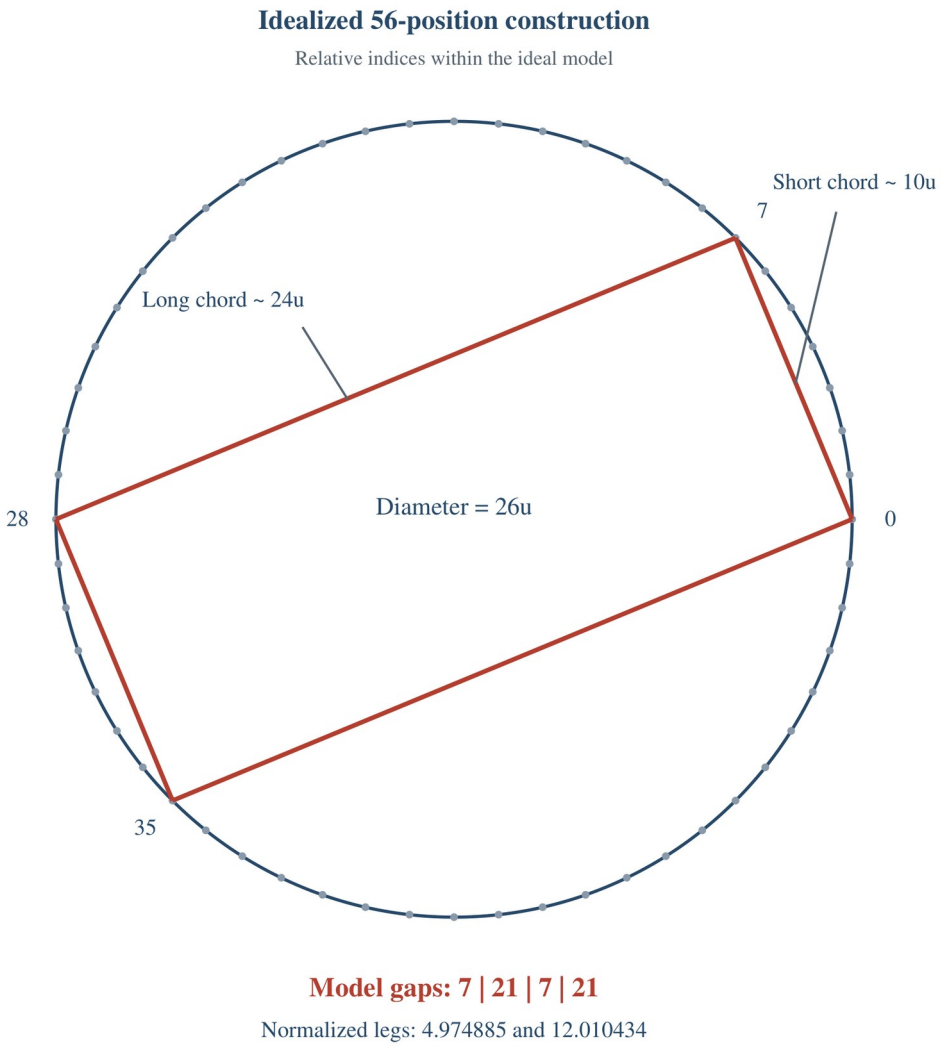


Figure S9.1. Idealized 56-fold Aubrey construction. Model gaps 7|21|7|21 yield chords close to the reduced 5:12:13 legs. The labels 0, 7, 28 and 35 are relative indices within the ideal model. Supplementary Notes 20–23 give the shape comparisons and the separate anchored-position test.

Among all 14 discrete templates, 7|21|7|21 gives the smallest shape residual in each archived plan convention after fitting a common rotation. The Cleal continuous gaps, 7.178|21.064|7.127|20.631 steps, round to the same sequence. In Cleal its angular RMS is 0.86°, compared with 2.81° for the next discrete template. The continuous 5:12:13 comparator gives 0.79°. At common centre, orientation and diameter, corresponding vertices of the two ideal models differ by 0.09 m. Supplementary Notes 20–23 and 32 distinguish these shape comparisons from registration with individual Aubrey positions.

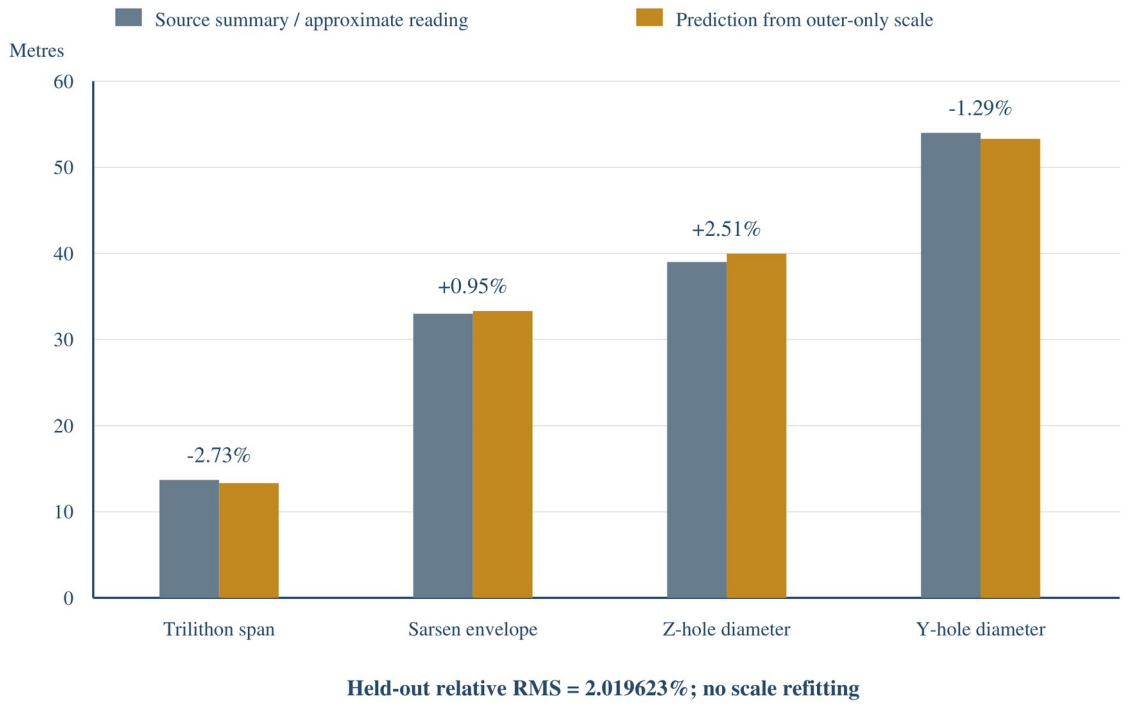


Figure S9.2. Four inner dimensions predicted from the outer Station–Aubrey calibration. Each prediction uses the same scale without refitting; the combined relative RMS is 2.02%.

In the declared metric-compression control, 72,285 of 1,000,000 perturbed configurations reach or improve the observed 2.02% RMS, a rate of 7.23%; the median simulated RMS is 4.12%. These results quantify the gain over the median and the frequency of comparable nearest-integer compression in this local ensemble. The frequency describes this stipulated perturbation process, not a probability for the full reconstruction or prehistoric intention (Supplementary Note 9).

The same length-transfer operations select 7|21|7|21 from all 14 discrete templates at fixed Aubrey diameter, with 2.12% RMS against 8.75% for the next template. Cutting the 10u by 24u rectangle along its 26u diagonal gives a right triangle with inradius 4u; half its long side is 12u, and diagonal minus short side is 16u. These operations express the existing Trilithon, Z-hole and Y-hole roles, respectively (main Figure 2). Together with copying the short side, they specify how each of the four inner lengths can be constructed from the outer triangle (Supplementary Notes 31–32).

The free circle fitted to the four Cleal Station proxies approximately matches the Aubrey centre and scale: its diameter is 86.49 m, and its centre lies 0.68 m from the separately fitted Aubrey centre. The 56 Aubrey proxies have radial RMS 0.63 m against that Station-derived circle. Alternative

sources, every Station omission and their sensitivity scenarios are retained in Supplementary Note 21.

Construction phases

Table S9.2. Construction-phase classification of inputs and held-out dimensions. Darvill et al.'s intervals are identified by event and source [2] (Table 3); the broader English Heritage dates are contextual summaries. These are external archaeological ranges, not uncertainty intervals from this model. Residual partitions retain the same outer-only scale (main Table 2).

Feature and model role	Archaeological phase	Consequence for the model
Aubrey circuit; A=56, diameter	Initial enclosure: 3000–2920 cal BCE in Darvill et al. [2] (Table 3); revised ditch ranges compared separately [18].	Only securely early count among A, B, C and D; its diameter alone does not calibrate the Station frame.
Station positions; D=4, short and long sides	Insecurely dated; assigned to Stage 2 (2620–2480 cal BCE) in the reconstruction of Darvill et al. [2] (Table 3).	Required for the 5:12:13 calibration and the four-count compiler; a date near the initial enclosure is unproved.
Sarsen circle and trilithons; B=30, C=10; two inner dimensions	Stage 2: 2620–2480 cal BCE [2] (Table 3); commonly summarized as c. 2500 BCE.	Two held-out roles: 2.05% RMS under the scale calibrated from Station–Aubrey dimensions.
Y and Z hole circuits; two inner diameters	Y/Z excavation: 1630–1520 cal BCE [2] (Table 3); broader heritage summary, 1800–1500 BCE.	Two held-out roles: 1.99% RMS under that same scale; their agreement cannot independently date an early plan.

The earthwork and Aubrey circuit belong to the early monument around 3000 BCE. Darvill et al.'s chronology assigns the major sarsen settings and Stations to Stage 2, 2620–2480 cal BCE, and Y/Z excavation to 1630–1520 cal BCE [2] (Table 3). The Station dating remains insecure, so their placement within that reconstruction is not an independent determination for each setting [1–3]. English Heritage summarizes the central stones as about 2500 BCE and the late holes more broadly as 1800–1500 BCE (https://www.english-heritage.org.uk/visit/places/stonehenge/history-and-stories/history/). Thus A=56 is the only securely early count among the four inputs at the nominal astronomical minimum. The Station-dependent calibration and all four inner comparisons cross phases (Table S9.2; Figure S9.3). These dates constrain structures; they do not date an otherwise undocumented design.

The temporal word alone also lacks a unique material inverse. Its map is $W=(A-B+C-2D, 3(B+D-C), A-B-C)$, a rank-three linear map with kernel generated by (1,0,1,1). Every positive integer inventory $(56+t,30,10+t,4+t)$, $t\geq -3$, gives the same W. With W fixed, the additional closure $r=D^2$ selects D=4 and t=0. This does not contradict the uniqueness theorem under all three closures; it identifies the extra assumptions that provide uniqueness. The theorem supplies conditional

mathematical identification, while independent archaeological evidence is needed to assign those assumptions to an early phase. A free common timing scale further makes proportional words indistinguishable under E (S5 Appendix, section 5).

Material component	Model role	Archaeological allocation
Aubrey circuit	**26u**	Early earthwork
Station frame	**10u by 24u**	Age uncertain in source set
Sarsen envelope	**10u**	Later central stone setting
Trilithon span	**4u**	Later central stone setting
Y-hole circuit	**16u**	Later activity
Z-hole circuit	**12u**	Later activity

Model roles across the monument's construction sequence.

Figure S9.3. Construction-phase dependency of the model roles. The Aubrey circuit belongs to the earliest monument; the sarsen settings and perhaps the Stations are later, and the Y/Z circuits later still. The figure locates features used in the mathematical reconstruction and does not imply that they were constructed together or that the proposed information was transmitted between phases.

S9.4 Constructive triangles, paths and directions

The pivot transformation converts the Station frame into the doubled 8:15:17 triangle through three length operations:

$T(10,24,26)=(26-10,(10+24+26)/2,10+24)=(16,30,34)$.

Requiring both input and output of this transformation to be right triangles forces the input ratio $y/x=12/5$. Its operations transfer the diagonal-minus-short-side difference, the semiperimeter and the sum of the legs. The input ratio is therefore required by the simultaneous right-triangle conditions, linking the two primitive families through one specified construction (Figure S9.4; Supplementary Note 36).

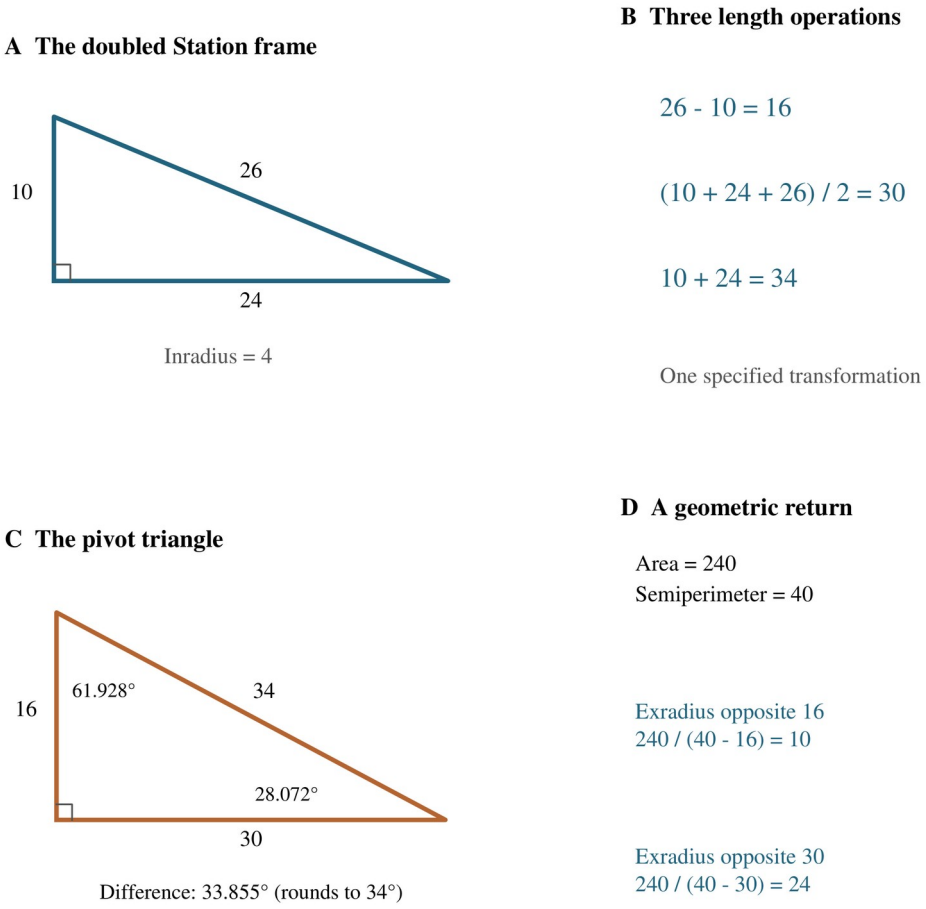


Figure S9.4. One transformation connects the two primitive triangles. The 10:24:26 right triangle supplies three operations that produce 16:30:34. Its pivot angles round to 28° and 62°, and their difference rounds to 34°. The inverse exradii recover the initial legs. All dimensions are model units, and both diagrams use local schematic axes. Approximate readings for the 7\|21\|7\|21 chord model are retained separately.

The resulting acute angles are 28.072° and 61.928°, and their difference is 33.855°. They round to 28°, 62° and 34° under the original rule. The ideal 7|21|7|21 version retains the 62/34 angular pair when its actual transformed triangle is used. A circle-based inverse returns the initial legs: the exradii opposite sides 16 and 30 are 10 and 24. Equal-area relations, Gaussian constructions and the distinct uses of 34 as a length and an angle label are derived in Supplementary Notes 36 and 52.

These constructions produce further quantities that can be compared with the plan. The four incentres of the Station rectangle's triangular halves have a circumdiameter of 53.72 m at the existing scale, close to the published 54 m Y-ring summary. The ordered paths J=x+y and V=2z+x realize 34 and 62; their two positive rectangular solutions are (10,24,26) and (78/7,160/7,178/7). Only the first returns integer inventories in the fixed module, and its external metric RMS is 0.26% against 7.93% for the other solution (Supplementary Notes 37 and 39).

A separate inventory-angle comparison gives arctan(30/56)=28.179°, only 0.096° from the recomputed stellar difference v−j=28.083°. The Aubrey–sarsen pair ranks first among all six inventory pairs under this same function. The derived ditch centreline is 32.12–32.19u under its declared boundary convention. These auxiliary comparisons, the complete tangent ranking and the modern constellation-boundary diagnostics are retained in Supplementary Notes 15–19 and 52.

Under the same equal-tension rule, the J route joins the midpoints of opposite short sides via one long edge, giving 5+24+5=34 in the ideal frame. The V route follows diagonal–short side–diagonal, giving 26+10+26=62. Under equal terminal tensions, these paths produce resultants along the short and long axes, respectively. Each channel thus has a length and a direction supplied by the same route. Applied to the Rees proxies, their axial azimuths are 52.15° and 140.04°: oblique axes with east–west and north–south predominance in the grid. The two channels therefore have distinct directional consequences under one stated operation.

The entrance can select these route families within the alternative directional protocol. J maximizes alignment with the normal to the 1–30 opening; V maximizes alignment with that normal's perpendicular. In both Rees conventions, the selected families have ideal-frame lengths 34 and 62 when their lengths are inspected after selection. This gives the entrance an explicit role in choosing which routes are read (Supplementary Note 40).

The two specifications exchange inputs and outputs. Under the entrance-based selector, the J–entrance alignment is the selection criterion and the ideal-frame lengths 34 and 62 are its outcome; under the length-based enumeration, the length labels and orthogonality are inputs and the alignments reported below are outcomes. Both read the same plan geometry and are not independent confirmations.

Under the length-based enumeration, the J path, labelled 34, gives an axis only 0.45° from the entrance normal in the primary digitization (axial Gram 0.99994). The V path, labelled 62, has mean Gram 0.93891 with the three available inner opening normals. These axes come from the specified outer-frame path decoder and are compared with the plan without fitting a rotation. In the indicative Station 91 branch the scores are 0.99988 and 0.93802 (main Figure 5; Supplementary Note 54). The inner-opening values average the three individual squared alignments; they do not score a single averaged normal.

The compact cross-Gram retains scores 0.0684 for J against the inner normals and 0.00084 for V against the entrance. The assigned and exchanged aggregate scores are 0.9694 and 0.0346. For exactly orthogonal channels, the exchanged score is identically 1 minus the assigned score. The digitized axes are nearly orthogonal: the two scores sum to 1.0040 in the primary branch and 1.0014 in the indicative branch. Their contrast therefore restates the alignment rather than providing an independent control (Supplementary Note 54).

The two channels also restrict each other within the declared route family. Two of its 12 ordered assignments recover the 34/62 length labels; only the short-side-midpoint J route paired with the diagonal–short-side–diagonal V route also produces orthogonal resultants. The alternative route of length 34 produces an axis parallel to V. In the digitized primary branch, the J–V axial Gram is 0.00136 for the selected pair and 0.99995 for that alternative. The ideal 7|21|7|21 form retains the selected pair, giving lengths 33.971 and 61.950, which round to 34 and 62 (Supplementary Note 54).

The three complete trilithon openings have normals closer to the Station long-side family than to its short-side family. Squared axial similarities are 0.984, 0.952 and 0.883 for the long sides, against 0.029, 0.032 and 0.146 for the short sides. No rotation is fitted, and the preference survives both Station 91 conventions and the stipulated ±0.25 m coordinate perturbations (Supplementary Note 35).

The Station-only construction predicts an axis 0.61° from the entrance normal, placing that pair first among 19 consecutive proxy pairs. With grid east fixed, the pivot rays approximate two trilithon-opening normals at 1.18° RMS; the discrete model gives 1.13°. References, reflections and assignments were selected retrospectively and are retained in full (Supplementary Notes 38–41).

The exhaustive 220-triangle proxy census finds 52–54–60 closest to 16:30:34 at 0.69% RMS with its own fitted scale. Across seven primitive comparators, 5:12:13 and 8:15:17 give the two smallest best-fit discrepancies, 0.56% and 0.69%. A different census retains 541 of 252,000 shape–orientation configurations under all six criteria, every survivor having the 7|21|7|21 form. The criterion-removal analysis shows that four restrictions select the same shape; direction adds a restriction, while the horizontal/vertical label adds none after it (Supplementary Notes 42–43).

These material and astronomical relations raise a further question: which parts of the reconstruction survive alternative assignments, inputs and scales? The next sections test stellar selection, early-versus-later phase preference, continuous metric targets and joint spatial–temporal performance. The closing sensitivity analysis identifies which physical readings depend on the source or convention.

S9.5 Regional stellar and word comparisons

Two controls preserve the original material assumptions within this same bright-star panel. First, an independently implemented absolute-RMS search holds W=(28,72,16) fixed across all 5,280 role classes, using a 1-year grid, local refinement and endpoint evaluation. Second, the 512 words are classified by whether any strictly positive integer inventory generates them under the unchanged compiler. For W=(d,m,r), let q=m/3 and h=(d−r)/2. Feasibility requires integer q and h and B=q+h>0; then D=t>max(0,−h), C=t+h and A=d+q+t provide every positive integer solution. This is weaker than imposing all three original closure equations. Both controls were formulated retrospectively after examining the unrestricted panel; their constraints come from the original map, and they do not test alternative compilers (S5 Appendix, section 3.1).

Spatially filtered stellar assignments

All seven temporal survivors in the principal V≤5 census lie in Cygnus. The expanded Hipparcos search supplies neither a named anchor nor Cygnus as input: 1,625 eligible stars across 77 regions yield 2,990 spatial candidates, of which seven reach or improve on the nominal temporal benchmark. Applying the ancient-contrast and Stage 1 filters jointly retains only Deneb–Sadr–Albireo–Aljanah–Fawaris in the declared roles. At V≤6, 1,072,375 spatial candidates yield 903 temporal passes and six joint passes, again all in Cygnus and all retaining Deneb and Sadr (Figure S9.5).

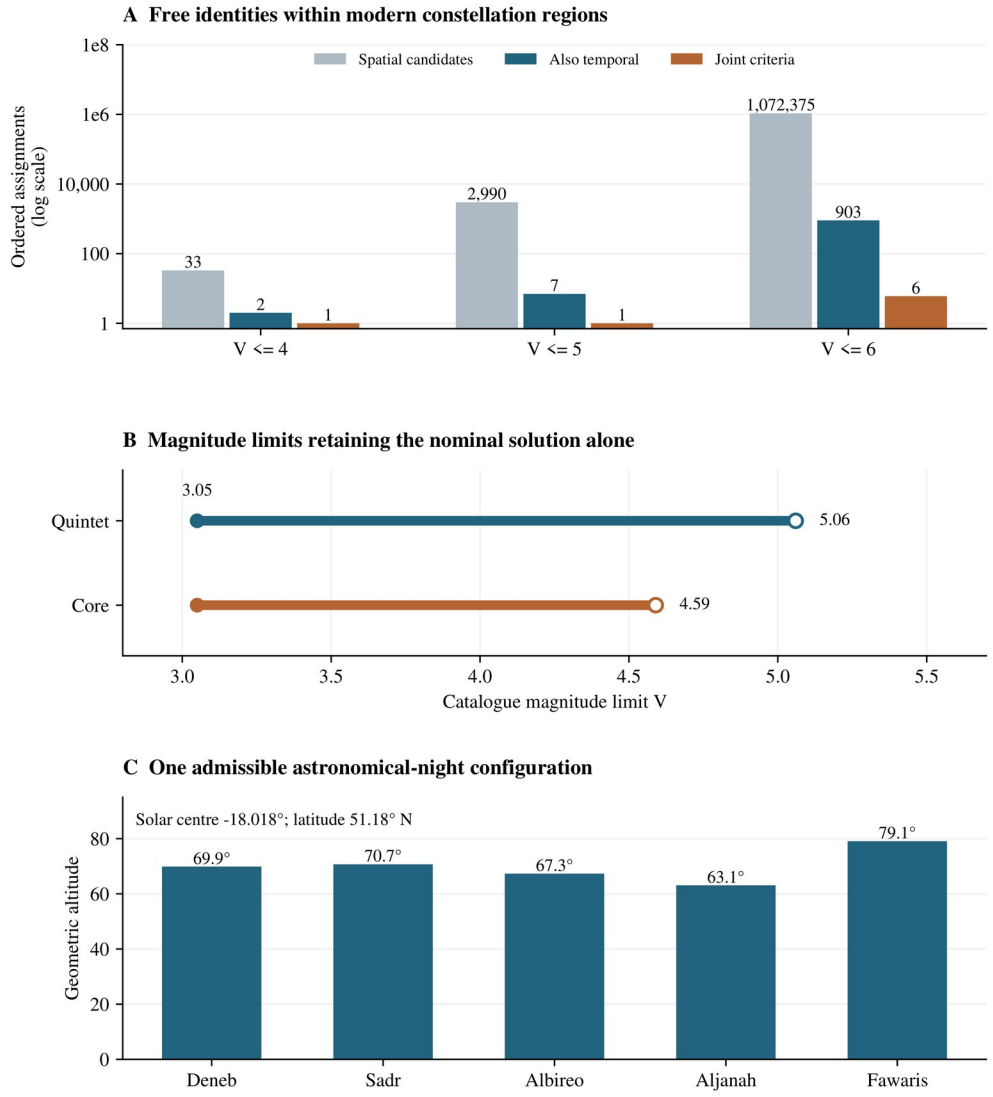


Figure S9.5. The joint stellar solutions concentrate in Cygnus and the nominal configuration is geometrically observable. Panel A reports the nested magnitude censuses after spatial and temporal filtering and after the additional joint contrast and Stage 1 filters. Panel B shows the full interval of magnitude limits for which the nominal quintet or ablated core is uniquely retained under its respective test. Panel C shows simultaneous stellar altitudes in an admissible astronomical-night configuration. The census uses uniform Hipparcos astrometry, and the night test allows season and sidereal time to vary.

The nominal quintet is brighter than every other joint survivor in at least one differing role and is never fainter in a corresponding role. Its role-ordered magnitudes are (1.25,2.23,3.05,2.48,2.86). It remains the unique assignment satisfying the unchanged joint criteria throughout the magnitude-limit interval $3.05 \le V < 5.06$ (Supplementary Notes 45–46).

Removing the latitude descriptor and third temporal channel leaves the Deneb–Sadr–Albireo core as the only temporal survivor at $V \le 4$. This core uniqueness spans limits $3.05 \le V < 4.59$ before ancient-contrast or horizon filters. There are five temporal survivors at $V \le 5$ and 131 at $V \le 6$. The core minimum is near 2848.4 BCE, compared with 2965.4 BCE for the full graph in the uniform catalogue convention, showing the third channel's contribution to the full phase (Supplementary Note 47).

All five selected stars can be simultaneously above 63° during astronomical night at the nominal uniform-catalogue phase. The flat-horizon annual-night calculation finds this configuration while the solar centre is below −18°. The same rule excludes two V≤5 core competitors containing stars that never rise at the site at their fitted epochs. This establishes a geometrically possible observing configuration and a physical distinction among candidates (Supplementary Note 48).

Earlier anchored censuses, both historical membership lists and every alternative assignment remain in the supplement. The expanded comparisons use Hipparcos positions propagated from catalogue epoch J1991.25, with nominal minimum 2965.4 BCE and RMS 0.390 minute. These are common-input comparisons; the primary archived specification remains 2965.2 BCE and 0.419 minute (Supplementary Notes 18, 27, 34 and 44–48).

Fixed word and released assumptions

With W=(28,72,16) and its original timing scale fixed, nominal Cygnus ranks first among all 5,280 role classes in the declared five-brightest regional panel, without spatial-tuple or archaeological chronology filtering. Its RMS is 0.390 minute; runner-up Reticulum gives 0.554 minute at 2848.6 BCE, 1.42 times the Cygnus RMS. This is sole first place within that panel, not a pass against an independently specified absolute threshold or a search of all stellar subsets (S5 Appendix, section 3.1). Expressed directly in degrees, the same Cygnus minimum has RMS 0.097532° against θ=(7°,18°,4°). The first-place ranking and the 1.42 runner-up ratio are identical under the angular formulation.

The crossed bright-star panel yields 336 qualifying classes after exchanging the final pair, equivalent to 672 labelled role-word descriptions across 57 regions. The common-catalogue Cygnus benchmark is 0.390 sidereal minute near 2965.4 BCE. Six classes have their best qualifying word-specific minima in 3000–2920 BCE: four Cygnus descriptions and two first/third-role reversals in Lacerta. The Lacerta example has W=(32,32,28), RMS 0.138 minute and minimum near 2921.5 BCE. The best timing fit anywhere in the panel is a Scutum description with W=(16,4,4), RMS 0.019 minute near 3237.2 BCE (Table S9.3). These alternatives are numerical comparators, not proposed ancient identifications. Their words, however, cannot arise from the original integer compiler: neither 32 nor 4 in the second channel can equal 3q for integer q. They are alternatives under word freedom, not counterexamples under the unchanged material map.

Of the 512 words, 55 admit some positive integer inventory under that map, defining 290,400 role-word classes. Algebraic feasibility retains 26 of the 336 timing passes. Only nominal Cygnus has its best qualifying minimum in 3000–2920 BCE. In the broader 2980–2720 cal BCE 95% ditch interval [18], three feasible classes remain: Cygnus and two Vela assignments with words (32,72,68) and (40,72,68), minima at 2905.8 and 2884.3 BCE, and RMS 0.365 and 0.276 minute. Both Vela assignments lie within the 2940–2800 cal BCE 68% interval, which excludes the unconstrained Cygnus optimum. Vela's r=68 cannot satisfy $r=D^2$ for integer D, so these are not full three-closure alternatives. All three chronology windows are reported rather than choosing the one with the strongest selectivity.

The free-scale primary Cygnus solution occurs near 2986.8 BCE with relative dispersion E=0.682%; the six-dimensional variant gives 2987.5 BCE and E=0.682%. In the common-catalogue comparison, Cygnus gives E=0.649% near 2985.5 BCE. Thirty-eight classes improve that value, placing Cygnus 39th; the 39 matching-or-better classes span 25 regions; Draco gives E=0.0206%

near 3052.0 BCE. Both grid resolutions recover identical qualifying candidate sets. The primary branch survives this scale change, but its exclusivity does not. Neither this panel nor the earlier separately conditioned censuses supplies a global chance probability or an equal-freedom comparison of complete archaeological models (S5 Appendix, sections 3–4).

Table S9.3. Comparison universes, fixed assumptions and released choices. All searches retain their stated stellar definitions and propagation model. Global optimization covers astronomical years −8000 to +2000. Absolute RMS and relative dispersion E are distinct objectives; their scores and ranks are not interchangeable. A “pass” uses the corresponding Cygnus benchmark, not an independent significance threshold. Interval membership after fitting and optimization within an interval are distinguished below.

Comparison and universe	Held fixed and varied	Objective and chronology	Result and location
S4 principal census Within-region subsets, V≤5	Fixed spatial tuple, W and timing scale; stellar identities and role assignments vary.	RMS; global epochs first. Ancient-contrast and initial-window filters applied afterward.	2,990 spatial candidates; seven temporal passes, all in Cygnus. Joint filters retain the nominal class (S9.5).
Fixed-word panel 5,280 role classes	Fixed W=(28,72,16) and timing scale; roles vary among five brightest stars in each of 88 regions.	RMS; no spatial-tuple or archaeological chronology filter.	Cygnus rank 1: 0.390126 min, 2965.4 BCE. Reticulum: 0.554285 min, 1.42× (S9.5).
Integer-feasible words 290,400 classes	Same bright-star panel and timing scale; 55 words vary under unchanged compiler feasibility, without all three closures.	RMS; global fitting, then interval membership. No spatial-tuple filter.	26 passes; one in 3000–2920 BCE and three in 2980–2720 BCE (S9.5).
Unrestricted library 2,703,360 classes	Fixed bright-star panel and timing scale; roles and all 512 library words vary. Compiler feasibility not imposed.	RMS; global fitting, then interval membership. No spatial-tuple filter.	336 passes in 57 regions; six classes in 3000–2920 BCE (S9.5).
Free timing scale 5,280 role classes	Fixed W and bright-star panel; role assignments vary and the common timing scale is fitted.	E; no spatial filter. Global search and separate interval-constrained searches.	Global: 39 classes match or improve Cygnus in 25 regions. Cygnus ranks 2, 2 and 4 in the three constrained windows (S9.5–S9.6).
Nominated-input sensitivity Three astrometric branches	Fixed Cygnus identities, roles and W; timing scale fitted. Primary, six-dimensional and common-catalogue inputs.	E; global search without archaeological chronology bounds.	Optima 2986.8, 2987.5 and 2985.5 BCE; E=0.6819%, 0.6817% and 0.6490%. These inputs do not rank a stellar panel.
Phase comparison Specified Cygnus model	Fixed word and roles. Original scale with channel-weight checks; separate tests fit scale under specified losses.	Global versus interval-constrained minima. Chronology explicitly bounds the latter.	Stage 2/original global RMS: 5.33× in the common catalogue. Free-E ratios: 15.31–16.06× across inputs (S9.6).

Comparison and universe	Held fixed and varied	Objective and chronology	Result and location
Metric-word extension Five targets, same panel	Fixed construction and calibration coefficients; targets derive from all five declared exterior conventions. Roles vary.	Fixed-scale RMS and free-scale E, separately; global and constrained searches.	Fixed-scale global rank 1 in all five variants, with optima in 3000–2920 BCE. Free-scale global ranks 10–49 (S9.6).
Joint space and time 5,280 classes; 10,560 typed assignments	Fixed S, W, reference and panel. Independent positive spatial and temporal scales; both final-pair spatial orientations.	Spatial CV or minimax with temporal E; no aggregate weight. Global and constrained comparisons.	No class dominates Cygnus. Global frontiers contain eight or six classes; no unique winner (S9.6).

The three constrained comparison windows are 3000–2920, 2980–2720 and 2940–2800 BCE, in that order; Stage 2 is 2620–2480 BCE. “Global” results do not use those intervals as fitting bounds. The complete panel definitions and adverse outcomes remain in S4 and S5.

S9.6 Chronology metric targets and adverse controls

Original target search and chronological comparisons

The inventory-derived word W=(28,72,16) ranks first by temporal fit among all 512 words in the declared material library, before applying an archaeological interval. Across the full 10,000-year search, its minimum occurs at 2965.2 BCE, with executed vector (27.785,72.653,16.233) sidereal minutes and RMS 0.419 minute, or 0.105°. The runner-up, (28,68,28), gives RMS 0.318° near 1744.1 BCE, approximately three times the primary RMS.

Three library words have minima in the declared 3000–2920 BCE initial-enclosure window; only W also has a fit at least as close as the primary result. The six-dimensional space-motion variant gives 2965.9 BCE. Main Figure 4 displays the complete search window and the archaeological comparisons (Supplementary Note 9).

The astronomical minimum falls within published radiocarbon-based intervals for the early monument, although those intervals do not enter the numerical minimization. It lies within Darvill et al.'s 3000–2920 cal BCE range for initial enclosure construction within Stage 1 [2] and Greaney et al.'s revised 2980–2720 cal BCE 95% ditch interval, but precedes the latter's 2940–2800 cal BCE 68% range [18]. These chronological models provide an external comparison with an early phase, rather than a date for the full input inventory. Any material system producing the same word under the specified operator would receive the same astronomical phase.

A solar comparison concerns the ideal cyclic construction. Its normalized long chord, $26\sin(21\pi/56)=24.0209$, is close numerically to the 24.0163° obliquity at the stellar phase. Under the degree-identification convention, solar inversion gives 3016.7 BCE in the primary model and 2999.4 BCE in the Laskar sensitivity model [30,31,45]. Of 416 disclosed cyclic arms, three intersect the obliquity range in the full window; only the selected arm gives a solution near the stellar phase (Supplementary Notes 10 and 25).

Phase comparisons

The fixed Cygnus model favours the early epoch over the later sarsen phase: the best fit in that phase has 5.33 times the RMS of the unrestricted minimum. In the common catalogue, the chronology-free optimum is 2965.4 BCE at 0.390 minute RMS. Restricting the same model to 2620–2480 BCE gives its lowest RMS at the oldest boundary, 2620 BCE: 2.080 minutes. The primary and six-dimensional inputs give corresponding ratios of 4.97 and 4.96 (Figure S9.6A). These input variants test astrometric sensitivity of one model, not independent archaeological confirmations.

The early epoch also outperforms Stage 2 channel by channel. At 2965.4 BCE, the common-catalogue absolute residuals are (0.211,0.605,0.213) minutes; the respective minima found anywhere in 2620–2480 BCE are (0.742,0.728,3.449), all at 2620 BCE. Every channel therefore favours the early reference date. Given these numerical interval bounds, any nonnegative channel weights with positive total preserve its lower weighted RMS, including when a channel is omitted. The primary and six-dimensional inputs give the same ordering. This establishes robustness of the phase comparison to weights, while allowing the weighted optimum to move to another epoch; it does not establish a new stellar ranking under changed weights (S5 Appendix, section 3.4). In the common catalogue, the narrowest margin is the Sadr–Albireo channel, 0.605 versus 0.728 minute; across all three input branches, the narrowest ratio is 1.040 in the six-dimensional branch.

The nominal optimum remains outside Greaney et al.'s 2940–2800 cal BCE 68% ditch interval. A separate constrained-epoch test gives Cygnus RMS 0.418 minute at its oldest boundary, 2940 BCE, only 7.20% above the unrestricted score (Figure S9.6B). Cygnus remains first among the same 5,280 fixed-word classes: every other class has an archived unrestricted minimum of at least 0.554 minute, and restricting its epoch cannot lower that minimum. Reticulum attains this bound at 2848.6 BCE, inside the interval, so it remains second with 1.33 times the constrained Cygnus RMS. This follows from the archived global scores and the new Cygnus bounded fit; it does not place the unrestricted optimum inside the narrower interval.

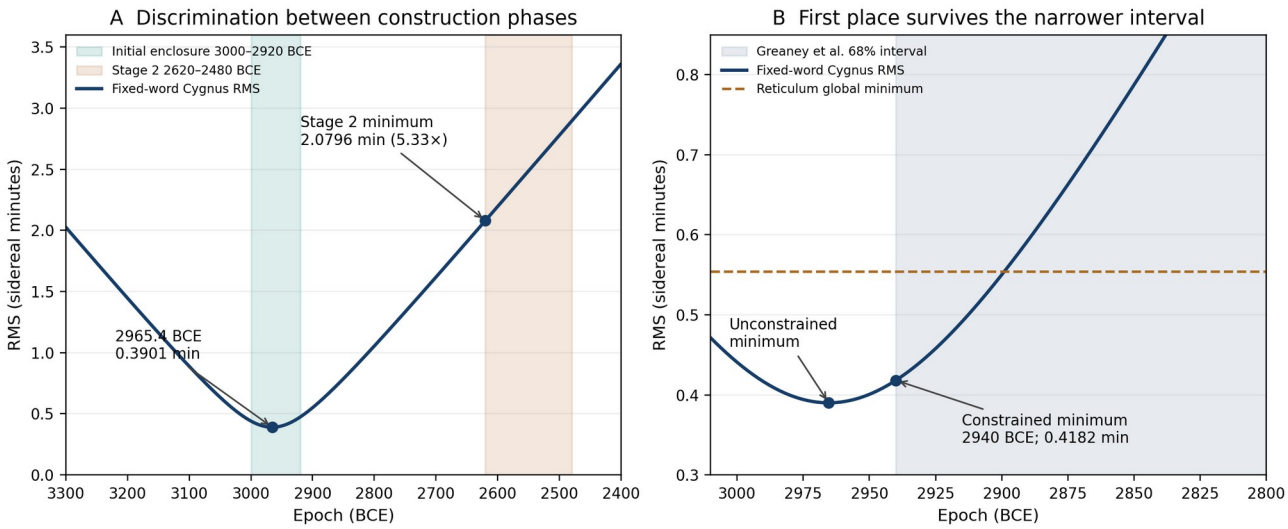


Figure S9.6. Temporal discrimination under the unchanged word and timing scale. Both panels use the common-catalogue absolute-RMS objective. (A) The unrestricted optimum falls in the initial-enclosure interval; the smallest error permitted in Stage 2 is 5.33 times the unrestricted minimum. (B) Restricting the epoch to the 68% ditch interval moves the Cygnus optimum to 2940 BCE while retaining a score below the best unrestricted score of every competing class. Reticulum's minimum lies within that interval, fixing its second-place score. Shaded bands show archaeological intervals, not probability densities. These retrospective constraints do not replace the chronology-free search in main Figure 4.

The constrained ranking shows that an optimum can fall outside an archaeological interval while retaining comparative fit inside it. It does not relocate the original optimum or remove the free-word and free-scale alternatives in section S9.5 (S5 Appendix, section 3.3).

The preference for the early branch also survives fitting a common timing scale under the tested losses. Across the primary, six-dimensional and common-catalogue inputs, the best Stage 2 relative dispersion E is 15.31–16.06 times the global minimum. In the common catalogue, even the best Stage 2 epoch and minimax scale leave at least one channel discrepant by 11.06%, whereas an epoch near 2998 BCE permits all three channels to agree within 0.794%. These results compare phases within the specified Cygnus model. They do not preserve its first-place temporal ranking when scale is freed: interval-constrained free-scale searches rank it second, second and fourth in the initial-enclosure, 95% and 68% windows, respectively (S5, sections 9–10).

Continuous exterior measures

The fixed-scale selection does not require the target to equal the exact integer word. Applying the specified construction to continuous exterior measures leaves Cygnus first among the same 5,280 role classes in all five declared variants (Table S9.4). The principal Aubrey convention gives Wmetric=(27.852,72.127,15.911), RMS 0.323 minute and an optimum at 2975.9 BCE. The five global optima span 2992.6–2960.6 BCE, all within 3000–2920 BCE, without using that interval in the global ranking (S5, section 12).

Table S9.4. Fixed-scale stellar selection under all five continuous metric conventions. Every row uses the common catalogue and the original numerical timing convention. The Aubrey diameters serve as diagonal proxies in the declared construction; the Euclidean diagonal is calculated from the two reported side means. Rank is within the 5,280-class panel. The range across variants is a sensitivity, not a confidence interval.

Exterior convention	Optimum BCE	RMS min	Rank
Aubrey 86.44 m	2975.885	0.322947	1
Aubrey 86.87 m	2964.122	0.424256	1
Aubrey 87.00 m	2960.577	0.459085	1
Aubrey 85.83168 m	2992.625	0.257887	1
Computed diagonal 86.79348 m	2966.211	0.404460	1

The five variants share measured inputs and the original construction. Their free-scale global ranks range from 10 to 49. All five fixed-scale global optima lie outside the 2940–2800 BCE interval; restricting to that interval reduces the MacKie variant to second place. The result establishes stability under the examined metric changes at the original timing scale, not under every timing convention.

Joint spatial and temporal scales

Cygnus remains nondominated in the joint spatial–temporal comparison when the two positive scales are fitted independently. Its spatial relative dispersion is 2.146% and its spatial minimax fractional error is 2.267%; its global temporal E is 0.649%. Cygnus belongs to frontiers of eight and six classes, respectively. It remains nondominated under both spatial criteria in each of the three previously examined archaeological windows (S5, section 11).

The spatial criterion alone ranks Cygnus second: a Vulpecula assignment improves spatial dispersion to 1.064% but has temporal E=4.075%. Conversely, candidates with lower temporal E worsen the spatial fit. This trade-off is the result of the joint comparison; nondominance does not identify a sole winner or supply a historical probability. The targets, stellar roles, J2000 reference and regional star selection remain fixed, and the diagnostic was formulated retrospectively after the separate rankings were known.

Source and model controls

The Aubrey-anchored assignment in the primary Cleal branch gives 8|21|7|20; exact registration with individual Aubrey positions remains unresolved. The continuous-gap and fitted-shape results above concern different observables. The tested eight-sector construction procedure and seven-hole residual model also fail to improve cross-validation over the regular-circle baseline (Supplementary Notes 20 and 30).

In the ancient mean ecliptic of date, the absolute stellar tuple is (11,35,63), and the unchanged inverse with r=16 returns (57,30,11,5). The rounded contrasts remain (24,28) at the tested phase. Fixed-J2000 stability therefore does not establish the same absolute register relative to the prehistoric ecliptic (Supplementary Notes 24 and 27). Changing the ideal cyclic solar input to the

exact 5:12:13 ratio or published mean-side ratio gives 2784.8 or 2713.2 BCE, respectively (Supplementary Note 25).

Several physical realizations are source-sensitive or unsupported. The four-incentre assignment to the 30 digitized Y symbols has 2.87 m RMS, with 97.13% of tested rotations matching as well or better. The path's equivalent force line crosses Stone 1 in the primary branch and clears the entrance only with indicative Station 91. The best 16:30:34 point triangle has a predominantly north–south long side, contrary to the proposed horizontal-long-side assignment. The ditch centreline is derived from width summaries; alternative boundaries do not preserve its integer reading (Supplementary Notes 15, 37, 40 and 42).

Selection depends on the declared comparison universe. Releasing Deneb in the historical contrast-only census leaves two assignments common to both lists. Among arbitrary positive integer words, 179 fit the nominated sky graph as closely as W. Its rank within the 512-word material library conditions on that graph. S5 separately reports unrestricted words, words feasible under the original integer compiler, and the original word held fixed. The fixed-word comparison ranks Cygnus first across its bright-star role panel without an archaeological chronology filter. These observations concern different candidate universes; none supplies a global historical chance probability (Supplementary Notes 9, 44–46 and 52; S5 Appendix).

S9.7 Regional geometric and dimensionless comparisons

The rule is applied to all 88 Hipparcos quintets at J1991.25 and J2000, and to all 88 archived HYG quintets. The selected Cygnus clock is then recomputed with the original word, scale and search window. Six archived kinematic scenarios test the common trio/quintet median, tree and role persistence at the existing clock epoch and at annual samples from 3000 to 1500 BCE. Catalogue membership and brightness ranks remain fixed. A subsequent scope check evaluates all 88 Hipparcos groups at three specified historical epochs. These are retrospective model checks; S6 records their order and complete results.

Cygnus is the only four-arm star-shaped minimum spanning tree in each 88-quintet catalogue panel. The geometric rule selects Deneb–Sadr–Albireo and leaves Aljanah–Fawaris as the remaining pair, recovering the existing temporal roles. At J2000 in the common Hipparcos catalogue, Albireo makes a 168.702° bearing angle from Deneb at Sadr, compared with 107.449° for Aljanah and 84.895° for Fawaris. No selected role changes between J1991.25 and J2000 in the 88 Hipparcos groups. Recomputing the clock with the recovered roles gives 2965.425 BCE and 0.390126 sidereal minutes RMS, reproducing the common-catalogue result in section S9.5. The original 5,280-class comparison and its 1.42 runner-up ratio remain the earlier regional benchmark; S8.9 reports the complete field census.

At that epoch, all six kinematic scenarios retain Sadr as a certified equal-weight spherical median of both quintet and selected trio, the four-arm tree and the same role assignment. The proportional change of the trio’s angular shape relative to J2000 is 0.0394–0.0472%. Across 1,501 annual epochs per scenario from 3000 to 1500 BCE, all 9,006 sampled model cases preserve both median certificates, the tree and the selected continuation; the minimum tree margin is 0.3990°. The additional 88-group checks at 3000 BCE, the existing optimum and 1500 BCE also leave Cygnus as

the sole four-arm case. S6 gives the certificates, scenario definitions, complete comparison panels and secondary Galactic-axis diagnostic.

With one geometrically selected assignment per group and no horizon or chronology restriction, Cygnus ranks second among 88 groups. Its minimum is E=0.649026% near 2985.482 BCE. Tucana ranks first at E=0.134236% near 3237.025 BCE, followed by Norma at 2.801116% near 7314.476 BCE. The Cygnus right-ascension intervals are (6.954903°,18.170633°,4.006198°); their common numerical scale is discarded. Every one of the 88 unrestricted scores reproduces its S5 free-scale value, and both search-grid resolutions recover the same minima. Table S9.5 distinguishes this panel from the unrestricted 5,280-role comparison in section S9.5.

Table S9.5. Leading dimensionless fits after the same geometric role rule. The last column reports the best score after reoptimization over epochs satisfying the necessary horizon condition. Scores are percentages; smaller is better. The search uses no archaeological date filter.

Group	Global E (%)	Global epoch (BCE)	Horizon E (%)
Tucana	0.134236	3237.025	None
Cygnus	0.649026	2985.482	0.649026
Norma	2.801116	7314.476	2.801116
Aquila	4.360427	2496.611	4.360427
Draco	4.623273	1299.828	4.623273

Seventy-one groups have at least one admissible epoch under the necessary horizon condition. Cygnus ranks first after reoptimization within all such epoch segments; Norma is second. Tucana has no admissible segment. Four of its five stars remain below the geometric horizon throughout the numerical search, with refined maximum upper culminations of −7.336°, −15.700°, −13.178° and −3.835°. At its best temporal fit, all five stars have negative upper culminations. Cygnus, in contrast, permits all five stars simultaneously above 64.719° near its optimum, at an appropriate sidereal time. The local-observation ranking therefore follows a common physical requirement rather than a chronology selection.

The dimensionless Cygnus optimum lies within the 3000–2920 BCE initial-enclosure interval, although it is just older than the separate 2980–2720 cal BCE 95% ditch interval. Within the later 2620–2480 BCE sarsen phase, its smallest E is 10.422720%, 16.059 times the global minimum. This reproduces the S5 free-scale phase contrast. The 2985.482 BCE optimum and the earlier fixed-unit 2965.425 BCE optimum are outputs of different objectives, not independent dates or uncertainty bounds. Across the full 5,280-role panel, free-scale alternatives remain as reported in section S9.5; the geometric selector specifies which one role assignment per group is retained here. The model still requires archaeological justification of the count map and any proposed transmission across phases.

S9.8 Information order execution and navigation

The public archive dated 26 August 2026 (Zenodo 22103786), with its Calanais extracts and checksum ledger retained in S5, records the stellar grammar, role order, rounding rule, W and

temporal operator. The Stonehenge map, dimensional ladder and subsequent diagnostics were developed with relevant data available. Archaeological dates do not constrain the original optimization or fixed-word ranking; explicitly labelled phase tests use them. S5 fixed-word and integrality checks followed its unrestricted panel, followed by phase and robustness diagnostics. S6 transferred the geometric selector after both stellar and Stonehenge results were known. S7 combined geometric roles, ratios and uniform horizon reoptimization after preliminary rankings and Tucana's horizon failure were known. S8 invariance and loss checks preceded the spherical axis audit, then the field census and kinematic recensus. The complete fixed-scale census and its matching free-scale comparison were executed after those four-arm results were known. Both field definitions and the angular target remain retrospective choices in this application. Radius calibration was formulated after the fixed-scale and free-scale census results were known; its two radius conventions and subsequent catalogue/state checks are additional retrospective analyses. These are retrospective tests, not preregistered discoveries. Supplementary Notes 1, 14 and 50–54 and the S5–S8 protocols retain their execution order and adverse outcomes, including rank losses and unsuccessful inverse constructions.

OpenAI ChatGPT assisted with literature retrieval, drafting, code construction and the additional S5 computational audits in September 2026; its exact model version was not exposed in the authors' working record. It also assisted with the October 2026 manuscript revision, S6–S10 computational diagnostics and reproduction checks. The code was executed against archived inputs, with checks and outputs supplied in the accompanying package. No archaeological survey or catalogue observation was generated by the service. Scientific interpretation and responsibility remain with the authors.

The complete fixed-scale and radius-calibrated field results are supplied in S8.9 and S8.10. The broader contextual report on Bulford (https://www.wessexarch.co.uk/Prototype-stonehenge-solar-alignment) is retained in S1 as source context; it is not a numerical input to the Stonehenge model. Revision v1.41 reorganizes the narrative and relocates extended analyses. It introduces no new numerical search or change to the archived candidate outputs.

Portable code, pinned inputs and complete numerical outputs support reuse [44]. The S5 README preserves the earlier execution history. For revision v1.35, the outer-scale calculation, local perturbation control and conditional integer audit were rerun, and the S5 checks recomputed reported temporal scores and verified archived ranks and robustness summaries. No new data or new full S2–S4 execution is claimed. Revision v1.36 adds the executed S6 diagnostic and its reproduction and integrity checks; the earlier S1–S5 archives and figure files are preserved unchanged. Revision v1.37 executes S7 and integrates its dimensionless comparison. All 88 roles and unrestricted scores are checked against S6 and S5, and both horizon-constrained and unrestricted minima agree across the two search grids. The earlier S1–S6 and figure archives remain unchanged. Revision v1.38 integrates the subsequently executed invariance, axis and field audits as S8. Their original numerical files and clean-extraction reproduction records are retained; all 26 field-census output files reproduced byte for byte before integration. Revision v1.39 independently enumerates the complete 19,939-group Hipparcos J2000 family and executes fixed-scale, free-scale and fixed-scale horizon searches on 1-year and 0.5-year grids. The earlier 03_Fields module was also rerun from clean extraction, reproducing all 26 outputs byte for byte. S1–S7 and figures remain unchanged. The packaging checks document claims and file integrity; no new

full execution of S1–S7 is claimed. Revision v1.40 integrates the executed radius-calibration audit and refits all four-arm candidates in four nominal and six targeted state panels under both radius conventions, with unrestricted and horizon-constrained searches on both grids. It checks candidate membership and roles, cross-grid scores, vector expressions and original-file integrity. The earlier modules and S1–S7 remain unchanged. Revision v1.42 adds the common-epoch dominance inference from archived complete-census minima and new Cygnus evaluations, including agreement across both grids and an independent vector check. It restores the dated public antecedent, separates the phase comparison in main 3.4, and updates the navigation of retained appendices. No new complete rival optimization or archaeological observation is claimed.

Revision v1.43 integrates the subsequent complete-pattern and unit-independent inverse analyses as S10 and main section 3.7. The added midpoint relation followed inspection of Cygnus. Both new complete censuses retain the archived field family and roles. S10 also reports the inconclusive construction-error diagnostic. The earlier S1–S8 numerical results and common-epoch dominance scope remain unchanged; the new objective is not added to that dominance proposition.

Revision v1.44 adds the matched free-midpoint/free-scale ablation and the equal-opportunity search over the previously archived 66 signed channel/divisor descriptions. These retrospective controls are reported in S10.3 and main section 3.7. Their ranks are 119 and 16 in the complete family; the 66-description comparison retains first place within the existing 283-field four-arm subset. Earlier numerical outputs are preserved.

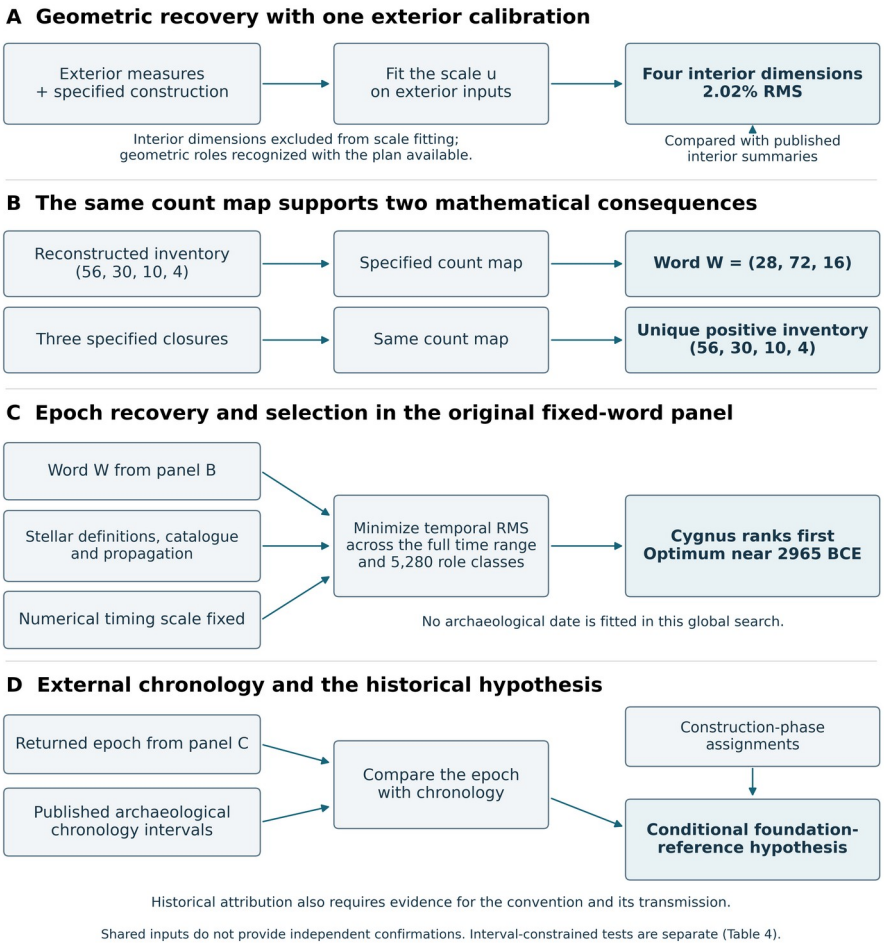


Figure S9.7. Dependencies of the original fixed-unit analysis. The exterior scale, count map, stellar search and chronological comparison occupy distinct steps. The 5,280-class panel shown here is the original regional comparison; the complete 19,939-field census and radius-calibrated extension are documented in S8.9–S8.10 and main Table 3.

Crosswalk for retained supplementary references

Earlier supplements retain their original numbering and numerical records. Use the following crosswalk when an earlier file cites a main-text location. References follow the v1.50 main bibliography. Reference_Crosswalk_v1_46.json maps older numbering; Reference_Crosswalk_v1_50.json adds the current shift of references 33–44 to 34–45. Earlier main Table 1 is now Table 2 and earlier main Table 2 is now Table 3; earlier main 4.1, 4.2 and 5 are incorporated in the unpartitioned Discussion. The main figures and the seven S9 figures together preserve all twelve earlier figures; S8 contains the detailed field tables. The crosswalk covers the earlier numbering through v1.40; v1.41 main 3.4 and 3.5 are now main 3.5 and 3.6. The new phase subsection is main 3.4, and the dominance proposition is S8.11.

Table S9.6. Navigation from the expanded v1.40 numbering.

Earlier location	Current location
Methods 2.1–2.2	Main 2.1; S9.1 and S9.4
Methods 2.3–2.6	Main 2.2–2.3; S9.2, S9.5–S9.6
Methods 2.7–2.10	Main 2.2–2.5; S9.7–S9.8; S6–S8
Results 3.1–3.3	Main 3.1–3.2; S9.2–S9.3
Results 3.4–3.5	Main 3.3–3.4 and Discussion; S9.3 and S9.6
Results 3.6–3.7	Main 3.6; S9.4
Results 3.8–3.13	Main 3.4 and 3.6; S9.5–S9.6
Results 3.14–3.15	S9.7; S6–S7
Results 3.16	Main 3.3 and Table 3; S8.1–S8.3 and S8.9
Results 3.17	Main 3.6; S8.4–S8.7
Results 3.18	Main 3.5 and Table 3; S8.10–S8.11
Tables 1, 3, 4, 5, 6	S9.1, S9.2, S9.3, S9.4, S9.5 respectively
Table 2	Main Table 2
Tables 7–9	Main Table 3 summarizes; S8.8, S8.1 and S8.9 retain detail
Figures 1, 3, 5, 6, 9	Main Figures 1–5 respectively
Figures 2, 4, 7, 8, 10, 11, 12	Figures S9.1–S9.7 respectively

S9.9 Construction alternatives and measurement decision bounds

The exterior-calibrated construction minimizes each absolute interior residual within an explicit operation library. This gives a comparison of alternative operations and assignments and a direct calculation of how far the input measurements can move before another prediction wins. The inputs and all earlier scientific results remain unchanged.

S9.9.1 Operation families and componentwise selection

Let (x,y,z)=(10,24,26). The exterior measurements (33.435,80.095,86.44) m give u=3.3314127219 m by the main least-squares rule. Interior values, ordered as sarsen, Z, Y and trilithon, are (33.0,39.0,54.0,13.7) m. The following library has 23 distinct numerical lengths.

Family	Operations
Sides and divisions	x, y, z; x/2, y/2, z/2; x/4, y/4, z/4
Differences and sums	y−x, z−x, z−y; x+y, x+z, y+z
Half-sums	(x+y)/2, (x+z)/2, (y+z)/2
Triangle constructions	(x+y−z)/2, xy/z, x^2/z, y^2/z, (x+y+z)/2

All 23×22×21×20=212,520 ordered assignments of four distinct entries are scored by relative RMS with u fixed. The adopted assignment (x,y/2,z−x,inradius) is first at 2.01962265%; replacing z−x by (x+y)/2 gives the runner-up at 3.10002440%. Each adopted length is also the unique closest library value to its own observation. Consequently the assignment minimizes every sum of those squared residuals with strictly positive per-feature weights. This assertion concerns diagonal weights; it does not assume or test a correlated survey covariance.

The systematic extension adds every positive absolute difference between the nine side, half-side and quarter-side lengths. After collapsing equal predictions it contains 42 lengths and 2,686,320 ordered assignments. The same four predictions are first, by the same componentwise argument and direct enumeration. Formula aliases are retained: for example, x−y/4 and the inradius both equal 4 on this frame. Numerical uniqueness does not identify a unique historical procedure.

Table S9.7. Comparisons at the unchanged interior inputs. The two free-scale rows use explicitly different estimators.

Comparison	Assignments	Rank	RMS %
23 lengths; exterior scale	212,520	1	2.01962
42 distinct lengths; exterior scale	2,686,320	1	2.01962
23 lengths; scale minimizes relative RMS	212,520	7	2.01709
23 lengths; metre least squares, relative-RMS score	212,520	6	2.03010
23 operations; measured sides and Euclidean diagonal	212,520	1	2.01410

S9.9.2 Exact decision boundaries and bounded sensitivity

For an adopted prediction p and adjacent competing lengths a<p<b, it is uniquely closest to a positive measured length m exactly when (a+p)/2<m<(p+b)/2. Relative and absolute residuals have the same nearest prediction for fixed m. If all four observations lie in their respective cells, the four distinct adopted predictions simultaneously attain the minimum. The intervals below therefore certify the assignment without assuming a probability distribution.

Table S9.8. Open measurement intervals preserving each adopted prediction at the fixed exterior scale. Endpoints are ties. Values are shown to three decimals; exact boundaries are archived.

Feature	23-length interval m	42-length interval m
Sarsen outer envelope	(32.033, 36.646)	(32.481, 34.147)
Z circuit	(36.646, 41.643)	(38.311, 41.643)
Y circuit	(49.971, 54.968)	(49.971, 54.968)
Trilithon span	(13.069, 14.991)	(13.069, 14.991)

The sharp uniform open-box limits for independent interior perturbations are 1.79317% in the primary library and 1.57190% in the extension (rounded; exact values are archived). Strict inequalities preserve each assignment. In the primary library the Y upper boundary is limiting; in the expanded library the sarsen lower boundary is limiting. These are limits on changes to the stipulated measurements, not estimates of their archaeological accuracy.

The exterior scale is a positive linear combination of the three exterior measurements. If each exterior input changes by at most δ in relative magnitude, u changes by at most δ while the ideal frame remains fixed. Requiring every interior input also to vary by at most δ gives a joint bound of 0.88862% in the primary library and 0.79217% in the extension (rounded). For a cell (L,U) at observed m, the bound is min[(m−L)/(m+L),(U−m)/(U+m)]. These bounds concern the fixed-frame calibration; the measured-side comparison is a separate branch.

Table S9.9. Exact ranges of the adopted construction's RMS over stipulated sensitivity boxes. All four interior values vary independently. Exterior variation acts through the fitted scale.

Interior variation	Exterior variation	RMS range %
±0.5%	±0.0%	1.56918–2.48862
±1.0%	±0.0%	1.15861–2.96758
±2.0%	±0.0%	0.44827–3.94159
±0.5%	±0.5%	1.56426–2.55162
±1.0%	±1.0%	1.15070–3.14686

At fixed scale and ±1% interior variation, the same assignment remains first in both libraries while its RMS ranges from 1.15861% to 2.96758%. The larger boxes report error sensitivity without asserting invariant rank. No empirical error distribution is supplied by the approximate interior source values. These intervals must not be read as confidence intervals or as probabilities of historical intention.

S9.9.3 Information order and reproduction

The libraries were specified retrospectively with the construction and measurements known. They compare alternatives conditional on the selected features, boundaries and exterior frame; they do not correct all prior analytical choices. Construction_Alternatives supplies the explicit formulas, all primary scores, aliases, analytic bounds and independent numerical checks. analyze.py regenerates the results; verify.py rereads every primary score, enumerates the expanded family, checks boundary equalities and box corners, and independently optimizes the sensitivity extrema.

Supplementary Material S6

Geometric recovery of the temporal roles

Lucas Giovani Ribeiro and Marcos André Simonssini
Supplementary Information | Stonehenge v1.47 | 30 October 2026

Operational definitions are given in main Methods. This section reports the associated results and derivations; executable instructions and the complete historical records are in Supplementary Data 1.

A geometric rule from the authors' separate stellar study recovers the role assignment already used in the Stonehenge temporal calculation. This appendix specifies the transfer, compares all declared candidates and tests structural persistence. The contribution is a geometric rationale for the roles; the clock result is reproduced with its original word and scale.

S6.1 Geometric roles

Table S6.1. Recovered roles in Cygnus

Selection step	Selected identity	Temporal use
Four-arm hub	Sadr (HIP 100453)	Shared vertex of the first two intervals
Brightest non-hub	Deneb (HIP 102098)	First endpoint
Most opposite bearing	Albireo (HIP 95947)	Third vertex
Remaining unordered pair	Aljanah (HIP 102488); Fawaris (HIP 97165)	Third interval

S6.2 Geometry and numerical certificates

Four-arm tree

Define $\Delta = \min_{ij}[d_{ij} - \max(d_{hi}, d_{hj})]$, over pairs of leaves. A positive Δ makes every non-tree edge longer than the longest edge on its tree path, so the four-arm tree is the unique minimum spanning tree. Calculations require $\Delta > 10^{-10}$ degree. An independently implemented Kruskal algorithm and the archived cycle-margin routine agree on all evaluated selections.

Shared median

For n equally weighted points including h, define $G_n = ||\Sigma_{i \neq h} u_{hi}||$, $S_n = \Sigma_i d_{hi}$ and $D_n = \max_i d_{hi}$. The reported global median certificate is $G_n \leq 1$ together with $C_n = 2S_n/n + D_n < 90°$. The first inequality is the vertex subgradient condition. For the distance sum $F(x) = \Sigma_i d(x,v_i)$, let $r = d(x,h)$. The triangle inequality gives $F(x) \geq nr - S_n$, whereas $F(h) = S_n$. Any competing minimizer therefore lies within $r \leq 2S_n/n$. The compactness bound places that whole ball within 90° of every input; there the distance sum is geodesically convex. The subgradient condition consequently certifies a global median at h. The noncollinear configurations here also give uniqueness. Apply this test separately to the quintet (n = 5) and the selected trio (n = 3).

S6.3 Census and unchanged clock

In both the 88-group Hipparcos panel and the 88-group HYG panel, Cygnus is the only four-arm star-shaped MST. No Hipparcos role changes between J1991.25 and J2000. In the common Hipparcos catalogue propagated to J2000, the Cygnus tree margin is 0.991432889°, G_5 = 0.305440349 and C_5 = 31.703110349°.

Table S6.2. Bearings from Deneb at Sadr, Hipparcos J2000

Candidate third vertex	Bearing separation
Albireo	168.702124°
Aljanah	107.448819°
Fawaris	84.894962°

Optimum: 2965.425144 BCE
RMS: 0.390126064 sidereal minutes
Interval vector: (27.789128708, 72.605468622, 16.213391853) sidereal minutes

This reproduces the common-catalogue result in main section 3.3. It is distinct from the primary-catalogue value near 2965.2 BCE and 0.419 minutes RMS. The roles are recovered geometrically; the time calculation, word and timing scale are unchanged.

Table S6.3. Comparison universes must remain separate

Comparison	Candidates	Cygnus rank	Runner-up / ratio
Original fixed-word temporal panel	5,280 role classes	1	Reticulum / 1.42
One geometric role per constellation	88 role classes	1	Boötes / 18.587778

Boötes has RMS 7.251576781 minutes in the restricted panel. Cygnus’s first place in a subset follows from its existing first place in the full panel. The larger restricted runner-up ratio is descriptive and supplies no new significance or strength multiplier. The 5,280-class comparison is the earlier regional benchmark; S8.9 contains the complete field census. Every selected class and score, including all alternative constellations, is retained in hipparcos_geometric_roles.csv.

S6.4 Persistence across the construction interval

At the existing 2965.425144 BCE clock epoch, all six scenarios retain Sadr as a certified median of the quintet and the trio, a strict four-arm tree and the same role assignment. Table S6.4 reports nominal diagnostics; scenario labels map to exact input keys below.

Table S6.4. Geometry at the existing clock epoch

Scenario	G_5	G_3	Tree margin (°)	Q (%)
HYG	0.386159	0.195987	0.403090	0.047226
Hip2 PM	0.386234	0.196063	0.404008	0.039443
Hip2 RV	0.386234	0.196063	0.404008	0.039443
HGCA PM	0.386375	0.196628	0.408379	0.040802
Albireo systemic	0.386210	0.196322	0.404349	0.044173
Deneb 802 pc	0.386210	0.196322	0.404349	0.044175

Compactness C_5 ranges from 31.732543° to 31.751814°; C_3 ranges from 31.128026° to 31.150968°, well inside the 90° sufficient boundary. Tree margins range from 0.403090° to 0.408379°. Full precision is in cygnus_epoch_metrics.csv.

Table S6.5. Annual scan from 3000 to 1500 BCE

Scenario	All 1,501 pass*	Min. tree margin (°)	Max. Q (%)
HYG	Yes	0.399024	0.047555
Hip2 PM	Yes	0.399948	0.039717
Hip2 RV	Yes	0.399948	0.039717
HGCA PM	Yes	0.404351	0.041086
Albireo systemic	Yes	0.400292	0.044481
Deneb 802 pc	Yes	0.400292	0.044483

* Both median certificates, the four-arm tree and the selected continuation persist. Across all six scenarios, maximum G_5 is 0.386957 and maximum G_3 is 0.196698 (upper-rounded); minimum tree margin is 0.399024°. The output construction_span_scan.csv preserves per-scenario maxima and minima.

Exact input keys: HYG; Hip2_PM; Hip2_RV; Hip2_HGCA_PM; Hip2_AlbireoA_systemic; Deneb_802pc_sensitivity. They represent HYG space motion, Hipparcos new-reduction inputs, updated axis-pair radial velocities, HGCA motions for Fawaris and Albireo, systemic Albireo A inputs, and the Deneb-distance sensitivity, respectively. They are targeted input substitutions, not six independent datasets.

S6.5 Additional scope and interpretation

Historical comparison scope

After the primary transfer diagnostic, the unchanged selector was applied to all 88 Hipparcos groups at 3000 BCE, 2965.425144 BCE and 1500 BCE. At each of those three specified epochs, only Cygnus has a strict four-arm MST. The 264 cases also agree after rotation into the precessed frame. These checks extend the finite catalogue comparison to the listed epochs; they do not establish uniqueness at every intervening year or over arbitrary stellar subsets.

Secondary Galactic-axis diagnostic

The archived forward Deneb-to-Sadr arc is the continuation from Sadr to the antipode of Deneb. Its minimum angular distance from the moving Sgr A* target at the existing clock epoch ranges from 0.836889° to 0.839731° across the six scenarios. Fixed-target results range from 0.836911° to 0.839752°. Both conventions remain in the output. The stellar manuscript reports a present-epoch value near 0.8654° for its baseline. This close approach does not isolate an epoch near 2965 BCE and is not used for role selection or temporal optimization.

What the transfer contributes

The rule supplies a compact structural rationale for the 3+2 organization: Deneb–Sadr–Albireo supplies the first two adjacent temporal intervals, while Aljanah–Fawaris supplies the third. The same central star and selected roles persist across all sampled construction-phase models. Intrinsic angular stability is compatible with changing right-ascension differences under precession; recognizable geometry need not imply a constant clock reading.

The five-brightest membership rule, original temporal roles and common-catalogue clock optimum already existed. The contribution here is the recovery and persistence of those roles under the transferred selector. It does not derive W, the timing unit, the ecliptic convention or a prehistoric tradition. Shared catalogue inputs and retrospective development prevent multiplication of these results as independent evidence. Main sections 3.3–3.7 retain the free-word, free-scale and adverse source controls.

Information order

The two manuscripts and their headline outcomes were available before this diagnostic was specified on 29 October 2026. The astronomy selector was reused unchanged. Primary protocol items A–C preceded this diagnostic execution; the historical 88-group extension was specified after the primary output and is recorded as an addendum. No date was reselected to improve the geometric descriptors. PROTOCOL.txt retains this ordering. The separate astronomy manuscript is unpublished.

S6.6 Reproduction and archive map

Table S6.6. Files and their evidential roles

File or directory	Content
inputs/hipparcos_panel.csv	Shared Stonehenge catalogue input
inputs/hyg_v70.csv; HYG_LICENSE	Archived HYG subset and catalogue terms
inputs/case_states.json	Pinned Cartesian states for the six scenarios
inputs/fixed_word_all_graphs.csv	Original 5,280-class score table
inputs/chronology_engine.py	Unchanged temporal/precession engine
astronomy_core.py	Archived stellar-selection and descriptor functions
results/hipparcos_geometric_roles.csv	176 rows: 88 groups at two epochs
results/hyg_geometric_roles.csv	All 88 HYG groups
results/cygnus_epoch_metrics.csv	Six scenarios at three epochs: 18 rows
results/construction_span_scan.csv	Six summaries of 1,501-epoch scans
results/historical_88_scope_check.csv	264 additional historical/rotation checks
PROTOCOL.txt; INPUT_PROVENANCE.json	Information order, source paths and hashes
SHA256SUMS.txt; verification/	Release integrity and execution evidence

The S1–S5 supplementary archive and figure archive accompanying the main manuscript are preserved byte for byte from v1.35. S6 is self-contained for its new calculations. It does not change the separate, previously disclosed source requirement for the third-party raster used by one S3 diagnostic. No new field survey data were obtained or assumed.

Reference: Ribeiro LG, Simonssini MA. Spherical certificates decouple centre and connectivity update times in evolving stellar patterns. 2026. Unpublished manuscript. Method provenance is recorded by source hashes; the required functions and numerical inputs accompany this appendix.

Supplementary Material S7

Dimensionless timing and the local horizon

Lucas Giovani Ribeiro and Marcos André Simonssini
Supplementary Information | Stonehenge v1.47 | 30 October 2026

Operational definitions are given in main Methods. This section reports the associated results and derivations; executable instructions and the complete historical records are in Supplementary Data 1.

The ratio formulation removes the assignment of an absolute time unit to an architectural count. The existing geometric selector recovers one role assignment per regional quintet before timing is evaluated. Cygnus ranks second among all 88 selected configurations, and first when the same necessary local horizon condition is applied with reoptimization to every group. The unrestricted minimum is near 2985.482 BCE. This appendix specifies the combined test and distinguishes it from the earlier fixed-unit and unrestricted-role comparisons.

S7.1 Ratios and invariance

The specified count map yields W=(28,72,16). Its ratio class is represented by w=(7,18,4). For role-ordered stars (1,2,3,4,5), define three nonnegative shortest right-ascension intervals relative to the equator of date: $d_1=|\mathrm{wrap}(\alpha_1-\alpha_2)|$, $d_2=|\mathrm{wrap}(\alpha_2-\alpha_3)|$ and $d_3=|\mathrm{wrap}(\alpha_4-\alpha_5)|$. Here wrap maps a degree difference into $[-180°,180°)$. The code uses degrees for convenience; no interpretation as a count-derived time unit is made.

Let $q_i=d_i/w_i$. Define $E=\mathrm{sd}(q_1,q_2,q_3)/\mathrm{mean}(q_1,q_2,q_3)$, with population standard deviation (divisor three). Report 100E as a percentage. E=0 exactly when d is a positive multiple of w. The objective is symmetric in the three relative channels. It equals the existing S5 free-scale relative dispersion, rather than introducing a new estimator. The main result is its combination with the geometric assignment and local horizon condition.

Unit invariance

For positive constants c and k, replacing d by cd and w by kw multiplies every q_i by c/k. Both the standard deviation and mean acquire this factor, so E is unchanged. Thus degrees, radians, sidereal minutes or seconds give the same objective, as do W and its reduced ratio w. Two independent ratios remain after common scale is removed. This does not eliminate the choice of count map, interval topology, loss function or equator of date.

The five-brightest regional membership rule and apparent-magnitude ordering come from the same Hipparcos panel as S5 and S6. The geometric rule uses angular distances at J2000: choose a strict four-arm tree hub when present, otherwise the angular medoid; choose the brightest other star, then the most opposite tangent-bearing endpoint, with the two remaining stars forming the final unordered pair. No group is excluded for lacking a four-arm tree. All 88 assignments are recomputed and checked against S6.

Angular relabelling and removal of scale

The fixed comparison can be written entirely in degrees. Let d(t) denote the three angular intervals, θ=W/4=(7,18,4) degrees, and Rθ(t)=RMS(d(t)−θ). The earlier code returns 4d(t) and compares it with W, so its RMS equals 4Rθ(t) at every epoch and for every candidate. The minimizers, ordering of candidates and ratio between their errors are therefore exactly invariant under this relabelling. The angular wording does not require interpreting the model as a claim that the builders used modern sidereal-minute terminology.

It still fixes an angular scale: one numerical unit becomes one quarter degree. The spatial tuple (10,34,62) also assigns degree readings to numerical labels, in the separate fixed-J2000 ecliptic construction. Because the Station count is D=4, the right-ascension target admits the notation θ=(W/D) degrees. This is an algebraically valid retrospective material parametrization. The equality D=4 does not independently derive the quarter-degree convention, the one-degree spatial convention or their prehistoric use. Changing angular units consistently preserves the calculation; changing the physical target scale changes the model.

Table S7.1. Fixed angular scale and scale removal are distinct operations

Operation	Cygnus epoch (BCE)	Full 5,280-role panel
Fixed target in sidereal minutes	2965.425	Rank 1; RMS 0.390126 minutes
Same target expressed in degrees	2965.425	Rank 1; RMS 0.097532 degrees
Ratios with relative dispersion E	2985.482	Rank 39; E=0.649026%

The 38 strictly better free-scale classes make Cygnus 39th, not 38th. Its preferred epoch moves by about 20.1 years when the fixed-scale RMS is replaced by the scale-free relative-dispersion objective, while remaining inside the 3000–2920 BCE initial-enclosure interval. This supports persistence of the preferred early branch under that change. It is not exact invariance to scale freedom, and the change of objective also changes the weighting of absolute versus relative errors. The later 88-assignment geometric comparison is a separate comparison universe.

The direct angular recomputation in audit_dimensionless.py recovers the archived fixed-unit optimum and RMS divided by four. The complete fixed-unit score table is retained as a benchmark. Earlier S1–S6 occurrences of “minutes” remain correct descriptions of their recorded coordinate units; their values do not need alteration to state the angular equivalence. The interpretive clarification here and in main section 2.3 governs the present revision.

S7.2 Search and uniform horizon reoptimization

Necessary condition for direct local observation

For every group, find the connected runs of positive horizon margin on the time grid. Refine crossings of $\min_i h_i = 0$ using bracketed root finding, then minimize E within every admissible segment. Endpoints on the zero-altitude boundary are retained as limiting infima. The calculation therefore allows a candidate with an invisible unrestricted optimum to compete at another epoch. Seventy-one of the 88 groups have a nonempty admissible segment; all their scores are supplied. Uniform application of this rule leaves Cygnus first and Norma second.

Additional diagnostics

For Cygnus and Tucana, maxima of each individual upper culmination are searched over the full interval with local refinement of all bracketed extrema and endpoints. A separate maximization over local sidereal angle finds the largest possible minimum altitude of the five stars at the unrestricted optimum. This establishes geometric simultaneity for Cygnus, without a night or season model. The original 2620–2480 BCE Stage 2 interval is also evaluated within the unchanged Cygnus ratio model.

The search is a numerical calculation under the specified catalogue and propagation assumptions. Agreement of the two grids and refinement of extrema support numerical stability; they are not a formal continuous-time certificate or a reconstruction of ancient photometry. The S6 tests of six kinematic scenarios concern role persistence and are not repeated here as six independent timing estimates.

S7.3 Comparison results

Table S7.2. Leading unrestricted ratio fits and horizon-constrained scores

Group	Global E (%)	Epoch (BCE)	Horizon E (%)
Tucana	0.134236	3237.025	None
Cygnus	0.649026	2985.482	0.649026
Norma	2.801116	7314.476	2.801116
Aquila	4.360427	2496.611	4.360427
Draco	4.623273	1299.828	4.623273

Cygnus retains the roles Deneb (HIP 102098), Sadr (100453), Albireo (95947), followed by Fawaris (97165) and Aljanah (102488) as an unordered pair. At 2985.482490 BCE, the right-ascension intervals in degrees are (6.954902530,18.170632926,4.006197656). E=0.006490264894, or 0.6490264894%. The reported precision supports numerical reproduction and does not represent archaeological dating accuracy.

Table S7.3. Comparison universes and what is held fixed

Comparison	Assignments	Result
Fixed unit and word	5,280 role classes	Cygnus first; about 2965 BCE
Ratios with free roles	5,280 role classes	Cygnus rank 39; Draco has a better assignment
Ratios with geometric roles	88 assignments	Tucana first; Cygnus second
Same geometric roles and local horizon	All 88 searched; 71 have an admissible epoch	Cygnus first; Norma second

The S5 Draco assignment with E≈0.0206% uses roles different from those selected geometrically. With the common geometric rule, Draco has E=4.623273% near 1299.828 BCE. This explains why restricting role choice changes the ranking; the broader free-role result remains valid. Restricting to the only four-arm tree would identify Cygnus before timing, so that filter is deliberately not used in this comparison.

In the Cygnus branch, the best Stage 2 value is E=10.4227203653% at 2620 BCE, 16.059006 times the unrestricted minimum. A second local minimum occurs near 6533.937 BCE at E=1.547060%. The early-enclosure result is the global minimum under the declared objective and search window, not the only local minimum.

S7.4 Horizon evidence and historical interpretation

Table S7.4. Tucana upper culminations at Stonehenge

HIP	At timing optimum (°)	Maximum over search (°)
110130	-23.596663	2.272376
1599	-35.570847	-7.335864
5896	-41.498998	-15.700163
2484	-39.073155	-13.178484
114996	-29.209278	-3.834995

At the Tucana timing optimum all five upper culminations are negative. Four remain negative even at their individually most favourable epochs in the full search, so there is no admissible epoch for the complete quintet. This is a large geometric separation from the horizon, not a marginal visibility decision. No extinction threshold was chosen to obtain the exclusion.

At the Cygnus optimum, the largest simultaneously achievable minimum altitude is 64.719137°, at local sidereal angle 259.606491°. All five stars can therefore occupy the upper sky together. The minimum of their individual upper culminations is 64.770471°, a different quantity. Neither figure claims an actual observing occasion.

The ratio optimum lies within the 3000–2920 BCE initial-enclosure range used in the main text, but is approximately 5.5 years older than the separate 2980–2720 cal BCE 95% ditch interval. The earlier fixed-unit optimum near 2965 BCE falls inside both of those intervals. Neither optimum lies inside the narrower 2940–2800 cal BCE 68% interval. These intervals are kept distinct. Archaeological dates never constrain the global fit or the local horizon condition.

Information order and remaining assumptions

The fixed-unit calculation, S5 free-scale results, S6 roles and their main outcomes were known before this integration. A preliminary cross-match found the second-place Cygnus result, then the Tucana horizon failure. The packaged protocol subsequently specified the uniform horizon reoptimization, regression checks, unit checks and complete output release. This is a retrospective robustness analysis. It cannot be counted as an independent confirmation of the chronology or converted into historical odds.

Removing the absolute timing scale answers the unit-convention objection for this branch. The map from architecture to 7:18:4, the regional five-star groupings, geometric selector and use of equator-of-date intervals remain substantive choices. An interpretation as prehistoric practice still requires evidence connecting those choices and their transmission with the monument. Positive geometric observability establishes possibility, not intention.

S7.5 Reproduction and provenance

Table S7.5. Reproducible archive

File	Purpose
audit_dimensionless.py	Geometry, timing, horizon search and unit checks
verify_release.py	Numerical scope, benchmarks and file-integrity checks
inputs/hipparcos_panel.csv	Shared catalogue positions, motions and apparent magnitudes
inputs/chronology_engine.py	Unchanged long-term precession engine
inputs/S6_roles.csv	Archived role-selection regression benchmark
inputs/S5_free_scale_scores.csv	All 5,280 archived ratio-score benchmarks
inputs/S6_fixed_unit_scores.csv	All 5,280 fixed-unit scores for angular equivalence
results/all_88_dimensionless.csv	Every unrestricted and horizon-constrained score
results/all_88_checks.csv	Every grid, score and rescaling check
results/summary.json	Full precision and detailed Cygnus/Tucana diagnostics
PROTOCOL.txt and INPUT_PROVENANCE.json	Information order, transformations and input hashes
SHA256SUMS.txt and verification/	Release integrity and execution records

Main Methods 2.3–2.5 and Results 3.3 report this comparison and its information order. Earlier S1–S6 archives remain unchanged; their section references describe their recorded versions. In particular, S6's fixed-unit result remains a reproduction of the earlier clock, whereas S7 supplies the dimensionless combined comparison. The unchanged precession implementation is documented by the Hipparcos and long-term precession references in the main manuscript. No new survey or telescope observation was obtained.

Supplementary Material S8

Stellar fields without constellation boundaries

Lucas Giovani Ribeiro and Marcos André Simonssini
Supplementary Information | Stonehenge v1.47 | 30 October 2026

Operational definitions are given in main Methods. This section reports the associated results and derivations; executable instructions and the complete historical records are in Supplementary Data 1.

The complete nominal Hipparcos J2000 census ranks Cygnus first among 19,939 fields under the fixed angular target (7°,18°,4°), without constellation boundaries or a four-arm entry filter. The matching free-scale control gives rank 68 with a nearby Cygnus epoch. Section 9 reports that extension. Sections 1–3 preserve the earlier cap-centred four-arm ratio panels and their targeted kinematic variants, whose robustness does not automatically extend to the new complete fixed-scale ranking. Sections 4–7 retain invariance and geometric-ratio diagnostics, including unsuccessful controls. All analyses are retrospective. Section 10 adds a distinct dimensionless calibration by each group's hub-centred angular radius, with complete nominal rankings and separately scoped four-arm sensitivity checks.

S8.1 Candidate family and recovered configuration

This family was selected after the Cygnus geometry and previous timing results were known. It is not a preregistered discovery, a multiplicity-calibrated significance test or an exhaustive enumeration of all five-star subsets. Unlike S7, it does not admit regional quintets centred only by a medoid. Thus its 256 nominal candidates are not a simple expansion of the earlier 88-group comparison; both are retained. The complete extension in section 9 also admits medoids, while retaining the cap-generation rule.

Cygnus roles are Deneb (HIP 102098), Sadr (100453), Albireo (95947), and the unordered pair Aljanah (102488) and Fawaris (97165). Reversing that final pair leaves the unsigned third interval unchanged. The centre is one of the five stars, so there are four nonzero hub distances.

S8.2 Nominal panels and timing results

Table S8.1. Every nominal field panel. R is the horizon-constrained runner-up error divided by Cygnus error.

Catalogue / geometry	Quintets inspected	Four-arm fields	Horizon fields	Rank global / local	R
Hipparcos / J2000	19,939	256	232	1 / 1	1.971
Hipparcos / 3000 BCE	19,904	267	243	1 / 1	3.890
HYG / J2000	19,939	255	231	1 / 1	1.679
HYG / 3000 BCE	19,923	261	237	1 / 1	3.888

Hipparcos gives Cygnus E=0.006490264894 at 2985.482490 BCE; HYG gives E=0.006490067261 at 2986.051275 BCE. Both construction epochs recover the same roles. The Hipparcos J2000 cap around Sadr retains the same five brightest members for radii approximately 16.238753–20.283777°. At 3000 BCE its interval is 16.225103–20.641986°. These intervals demonstrate membership over a range of radii, rather than a single radius chosen from temporal fit.

The nominal global runner-up is centred on HIP 109268. In Hipparcos it reaches E=0.006590907555 at 1582.263739 CE, only 1.5507% above Cygnus. This small global margin must be reported alongside first place. The regional name associated with this star is not an input to generation.

In every nominal panel, Cygnus remains first at nested ceilings V≤4, 5 and 6, with and without the horizon condition. In Hipparcos J2000 these have 22, 66 and 256 candidates, of which 19, 59 and 232 have admissible epochs. The lower ceilings are obtained by restricting the faintest member: stars dimmer than that member cannot displace a brighter top-five set.

S8.3 Targeted kinematic sensitivity and comparison scope

Table S8.2. Six complete recensus variants. E is Cygnus relative dispersion; R is the local runner-up/Cygnus error ratio.

Variant	Global rank	Local rank	E (%)	Epoch (BCE)	R
Archived HYG states	1	1	0.649012	2986.053613	1.679
Hip2 proper motion	1	1	0.653522	2986.973039	1.667
Hip2 radial velocity	1	1	0.653521	2986.973037	1.667
Hip2 with HGCA	2	1	0.661960	2985.499905	1.646
Albireo systemic motion	2	1	0.690059	2984.946520	1.579
Deneb 802 pc sensitivity	2	1	0.690059	2984.946533	1.579

The local first-place result survives all six targeted variants, with the smallest margin 1.5789. Global first place does not: Cygnus is second in the final three rows. The range 2984.95–2986.97 BCE measures sensitivity to these state substitutions under a fixed objective and background catalogue. It is not a confidence interval and does not replace the broader loss sensitivities. S6 provides the state definitions and provenance; these are six targeted catalogues, not six independent complete surveys. The archived HYG state row differs slightly from the nominal HYG census because its Cygnus states come from the pinned S6 state file.

Table S8.3. Candidate families remain distinct

Family	Choices retained	Cygnus result
S5 fixed-unit roles	5,280 regional role classes; original angular scale	First near 2965 BCE
S5 free-scale roles	Same 5,280 classes; relative-dispersion loss	39th near 2985 BCE
S7 geometric roles	88 regional quintets; tree hub or medoid	Second globally; first among 71 horizon-admissible groups
S8 geometric fields	No regional boundary; star-centred cap and four-arm tree	First in four nominal panels; local first in all six state variants

The field census eliminates regional boundaries as a prerequisite for this recovery. It retains the count map, ordered target, five-member field definition, brightness and role rules, loss, astrometry and search window. Its candidate counts and error ratios are descriptive comparisons, not historical odds. Tucana’s earlier regional result remains valid under its own rule; the new field family is not used to erase it.

S8.4 Coordinate invariance and the relative loss

The preceding invariance audit concerns the S7 assignments and supplies an algebraic interpretation applicable to the same intervals in S8. Let u_i and u_j be unit stellar directions and k the unit physical terrestrial pole at the epoch, all expressed in one common frame. Define the scalar $a=u_i\cdot u_j-(u_i\cdot k)(u_j\cdot k)$ and $b=|k\cdot(u_i\times u_j)|$. Then $d_{ij}=\mathrm{atan2}(b,a)$ is the absolute shortest longitude interval about k, between zero and π. This is the right-ascension interval, not the great-circle separation. If an equatorial projection vanishes, longitude is undefined; no tested input encountered this case.

A common orthogonal change of basis of u_i, u_j and k preserves a and b, including reflections. The formula therefore requires neither a right-ascension zero nor chosen equatorial x and y axes. It retains the physical pole and its precession. The audited implementation agrees with direct right ascension to approximately 1.65×10^{-11} degree over all 88 assignments and 20,001 epochs. Twenty-four orthogonal basis changes at eleven epochs per group agree to approximately 5.02×10^{-11} degree. These checks verify the implementation of an algebraic invariance already implicit in right-ascension differences.

A fitted common scale

Write $q_i=d_i/w_i$ with w=(7,18,4), and relative residual $r_i=sq_i-1$ for a positive common inverse scale s. Minimizing the mean squared residual gives $s^*=\Sigma q_i/\Sigma q_i^2$. Its minimum is $F_2^2=1-\mathrm{mean}(q)^2/\mathrm{mean}(q^2)$. Since $E^2=\mathrm{mean}(q^2)/\mathrm{mean}(q)^2-1$, it follows that $F_2=E/\sqrt{(1+E^2)}$. This transformation is strictly increasing, so every ranking and epoch minimizer is unchanged. Numerical disagreement between the two forms is at most 3.33×10^{-16} in the archived test.

This establishes that the chosen dispersion is equivalent to fitting a common inverse scale with a quadratic relative-residual loss. It does not specify a probabilistic measurement-error model. Multiplying all angles by a positive constant changes s but leaves E and F_2 unchanged. The fixed target in degrees and the earlier target in sidereal minutes instead differ only by unit conversion; freeing scale changes the objective and can change rankings, as recorded in S5–S7.

Conditional norm and weight bounds in the regional panel

For each of the 71 horizon-admissible S7 groups, define U_p as the infimum over admissible epoch and positive scale of the p-norm of r. The archived numerical minima give $F_2(\mathrm{Cygnus})=0.006490128202$ and $F_2(\mathrm{Norma})=0.028000182275$, with Norma the runner-up and R=4.314272600. In dimension three, norm equivalence bounds the competitor/Cygnus ratio below by $R/\sqrt{3}$ for all $1\le p\le\infty$. This is greater than one, preserving first place throughout that family, conditional on the stated numerical minima.

For positive common channel weights λ_i summing to one, $\sqrt{(3\lambda\min)}F_2\le F\lambda\le\sqrt{(3\lambda\max)}F_2$, after minimizing over the same domain. A sufficient condition preserving first place is $\lambda\max/\lambda\min<R^2=18.612948070$. A ratio at most 18 therefore suffices. This excludes zero weights, group-specific weights and retrospective choices of a different weight vector per competitor. These margins belong to the old regional panel; they are not transferred to the new field family.

S8.5 Loss controls and continuous spatial reconstruction

Table S8.4. Direct loss reoptimization in the 71-group horizon-admissible regional panel

Relative-residual loss	Cygnus rank	Cygnus optimum (BCE)
Mean absolute residual L1	1	2973.112856
Root mean square residual L2	1	2985.482485
Maximum absolute residual Linf	1	2997.928665

All three sampled-loss optima lie in the cited 3000–2920 BCE initial-enclosure interval. The norm bound concerns rank, not constancy of epoch for every p. Numerical minima agree across 0.5-year and 1-year grids with local refinement; they are not interval-certified global optima. The epoch span in Table S8.4 is a sensitivity result, not an archaeological uncertainty distribution.

Releasing the number-to-interval order

Allow every group all six permutations of 7:18:4, reoptimizing epoch and scale under the same horizon rule. There are 528 group-order combinations, 426 admissible. Rank each group by its best ordering. Lyra becomes first with 18:4:7, E=0.002880093148 at 1766.714456 CE. Cygnus is second and retains 7:18:4, E=0.006490264894 near 2985.482481 BCE. No chronological filter is added to remove Lyra. This exposes the role of the ordered map; it does not invalidate the result when that map is retained. The complete permutation control belongs to the regional family and has not been repeated as a full field-family permutation census.

Removing the ideal triangle and Aubrey calibration

Table S8.5. Continuous exterior construction and held-out interior summaries

Interior role	Construction	Output (m)	Published (m)
Trilithon span	(x+y−z)/2	13.368260	13.7
Sarsen outer diameter	x	33.435000	33.0
Z-hole diameter	y/2	40.047500	39.0
Y-hole diameter	z−x	53.358480	54.0

The root-mean-square relative discrepancy is 2.014104407%, close to the original 2.02%. This preserves dimensional agreement without imposing an integer triangle or an Aubrey diameter. It uses two exterior measures to set shape and scale, whereas the original fixed shape used one estimated scale. The slight reduction is not a statistical improvement under equal parameter counts. Rounded inputs, feature boundaries and retrospective assignments remain shared.

With r=y/x, dividing every output by x gives $[(1+r-\sqrt{(1+r^2)})/2, 1, r/2, \sqrt{(1+r^2)}-1]$. This is a dimensionless expression of the same continuous construction. It does not add independent observations or establish historical transmission.

S8.6 Spherical axis and centre ratios

Here a=d(Deneb,Sadr), b=d(Sadr,Albireo), c=d(Sadr,Fawaris), e=d(Sadr,Aljanah), ℓ=d(Deneb,Albireo) and τ=d(Fawaris,Aljanah), where d is great-circle distance. These symbols are local to this comparison and are not inventory counts.

Table S8.6. Great-circle geometry at the imported ratio optimum 2985.482485 BCE

Quantity	Value
a, b, c, e (degrees)	6.131807, 16.225142, 8.406342, 8.010386
ℓ, τ (degrees)	22.270452, 16.219591
b/τ	1.000342250
ℓ/τ	1.373058775
Normalized radii a, b, c, e	0.158143542, 0.418457669, 0.216805382, 0.206593407

The Sadr–Albireo arm exceeds the transverse width by 0.034225%. This near equality was noticed while inspecting the distances; it was not a prediction made before examining Cygnus. Apply the same |log(b/τ)| score to all 88 geometric regional groups at the same imported epoch. Cygnus is first, with runner-up Capricornus error 37.684 times larger. It remains first at every half-year sample in 3000–2920 BCE, with minimum runner-up ratio 33.191. At J2000 it is second. These ranks condition on the chosen relation and common epoch.

Two adverse controls delimit that finding. Allowing each group its closest equality among all 15 pairs of the six distances puts Cygnus second at the imported epoch and eighth at J2000. Allowing each group to choose an epoch gives exact b/τ=1 crossings in Cancer at 6601.718 BCE, Cygnus at 3526.377 BCE, Cetus at 1058.161 BCE and Capricornus at 1357.933 CE. Thus the relation does not provide a second clock confirming 2985 BCE.

The complete HYG regional panel also places Cygnus first at the imported epoch and second at J2000. Across the six S6 Cygnus state variants, the fixed-epoch mismatch ranges from 0.021921% to 0.118501%, while exact-equality epochs vary from approximately 3323 to 5329 BCE. Those six checks change Cygnus only, unlike the full field recensus in section 3. No six-variant all-sky ranking is attributed to this axis test.

The Station side ratio is 80.095/33.435=2.395543592, versus ℓ/τ=1.373058775. Reading the two stellar axes as rectangle sides misses the ratio by −42.683%; reading them as its two diagonals requires equality and misses by +37.306%. A centred rectangle also has four equal centre-to-vertex distances, whereas the stellar radii differ by a maximum/minimum factor 2.646. These two explicit proportional templates fail. No flexible projection was fitted to rescue them.

In the right-ascension channel, (7+18)/4=6.25 and 7/(7+18)=0.28 merely restate the target’s axis ratio and hub position when the adjacent intervals add. They are not the great-circle quantities above and cannot be counted as further independent matches. The spherical near equality adds a descriptive property of Cygnus, without identifying a new homologous feature in Stonehenge.

S8.7 Inverse construction and withheld-channel controls

A further retrospective test inverts the existing continuous construction, with an irrelevant positive common scale omitted: $(d_1,d_2,d_3)=(2z-y,3y,z-x)$. The inverse is $y=d_2/3$, $z=(d_1+y)/2$ and $x=z-d_3$. The right-angle condition $z^2=x^2+y^2$ is equivalent to $9d_1d_3+3d_2d_3-9d_3^2-d_2^2=0$. Retain only positive dimensions with $x<y$. These are conditions on a hypothetical inverse rectangle, not a new survey measurement.

For every one of the 256 Hipparcos J2000 fields, search all sign-changing roots over the full time window with 0.5-year and 1-year grids and bracket refinement. Both grids return 21 valid roots in 14 fields. This scope does not certify the absence of tangential roots or crossings missed between grid samples. Compare the inferred y/x afterward with the published 2.395543592; neither the aspect nor chronology selects the candidates.

Cygnus has a root at 2936.745850 BCE giving y/x=2.551117104, 6.4943% above the published aspect. This is the closest of the 21 retained roots, but it is not precise metric recovery and does not improve the earlier dimensional fit. Its other root is near 6703.491 BCE with aspect 2.846313370, a discrepancy of 18.817%. The complete root table is supplied; the inverse is not used to alter the field census or counted as an independent positive result.

Fitting two channels and inspecting the third

An auxiliary Cygnus test equates each pair of normalized intervals and inspects the unused channel. The first two channels never reach exactly 7/18 in the sampled full window; their ratio spans approximately 0.36128–0.38295 against 0.38889. Fitting channels 1 and 3 returns roots near 6498.313 and 2997.929 BCE, leaving channel 2 discrepant by +3.7973% and +1.6004%. Fitting channels 2 and 3 returns roots near 6573.388 and 2973.113 BCE, leaving channel 1 discrepant by −3.7844% and −1.5794%. All roots and residuals are retained.

These calculations expose multiple roots and imperfect third-channel agreement. The two fitted ratios reuse the same inputs and target, and the control was designed after the full fit was known. It is therefore a sensitivity diagnostic rather than prospective validation of a withheld observation.

What the combined audits establish

The dimensional agreement survives a continuous exterior construction. The ratio objective has a coordinate-invariant form about the physical pole. A specified brightness-and-field census recovers the five-star group without regional boundaries: fixed-scale Cygnus rank is 1 in the complete 19,939-group census, whereas free-scale rank is 68 there and 1 in the four-arm subsets. Local ratio ranking survives the targeted state variants within the cap-centred four-arm family. Radius calibration links extent and equatorial intervals without a fixed degree-per-count conversion; its complete-census rank depends on radius convention and its local inference uses a necessary horizon condition. Five-member star-centred circular fields, the ordered count map and geometric roles remain model choices. None of these comparisons establishes prehistoric use, transmission or a construction date; ranks are not independent probabilities.

S8.8 Reproduction and integration record

Table S8.7. Run commands from each named module directory in Supplementary Data 1.

Directory	Commands in order
01_Invariance	python audit_robustness.py
02_Axes	python audit_axes.py python audit_kinematics.py
03_Fields	python all_sky_caps.py python kinematic_fields.py python diagnose_inverse.py
04_FixedScale	python audit_open_fields.py 1 python audit_open_fields.py 0.5 python verify_results.py
05_RadiusCalibration	python radius_normalized.py 1 python radius_normalized.py 0.5 python radius_dynamic.py 1 python radius_dynamic.py 0.5 python check_invariants.py python check_dynamic_invariants.py python check_horizon_winner.py python robustness_panels.py 1 python robustness_panels.py 0.5 python verify_radius.py

No original georeferenced Station or Aubrey survey was obtained. These calculations use existing measurements and astrometry and require no further archive response.

S8.9 Complete fixed angular census and matched free-scale control

This extension was executed after the four-arm ratio findings were known. It uses the same archived nominal Hipparcos V≤6 catalogue, angular proper-motion model, precession engine and geometric selector. Independent cap enumeration returns 19,939 distinct quintets across 25,161 generating radius intervals. The centre remains among the five brightest entries in each generating field. This is the complete family under that definition, not all five-star subsets of the catalogue.

At J2000, each quintet receives one assignment: unique four-arm minimum spanning tree hub if present, otherwise angular medoid; brightest non-hub endpoint; most opposite tangent-bearing endpoint; remaining unordered pair. The last pair is stored in increasing HIP order without changing its unsigned interval. Of the 19,939 groups, 283 have a unique four-arm hub at any member; 256 additionally have that hub among their generating cap centres. The latter assignments exactly match the archived 03_Fields panel after canonicalizing the residual pair.

For absolute wrapped right-ascension widths d(t) in degrees and θ=(7°,18°,4°), minimize $R(t)=\sqrt{\{\Sigma_i[d_i(t)-\theta_i]^2/3\}}$. Here R denotes angular RMS; the R columns in Tables S8.1–S8.2 denote error ratios. Then 4R is the numerical RMS in quarter-degree units, equivalent to the original sidereal-minute representation of W=(28,72,16). Conversion of units is exact and leaves ranks and epochs unchanged; choosing an absolute target is still a model assumption. The matched free-scale search minimizes the same E defined in section 2 over exactly the same role assignments.

Both objectives are searched over astronomical years −8000 to +2000 on 1-year and 0.5-year grids, refining every bracketed minimum and endpoints with the archived optimizer. The fixed-scale horizon branch locates and refines all intervals in which every member has positive geometric upper culmination at latitude 51.18° N, then reoptimizes R within them, including boundary infima. Neither catalogue grouping nor optimization uses archaeological chronology. Groups and roles are held fixed during their temporal searches.

Table S8.8. Nominal Hipparcos J2000 complete census and subsets. Error ratio is runner-up/Cygnus under the stated objective; a dash indicates that Cygnus is not first. Only the explicitly labelled row imposes the horizon condition.

Objective and candidate family	Groups	Cygnus rank	Error ratio
Fixed target; all fields	19,939	1	2.201
Fixed target; horizon reoptimized	17,860	1	2.626
Fixed target; four arms, any hub	283	1	12.915
Fixed target; four arms, cap-centred hub	256	1	12.915
Free scale; all fields	19,939	68	—
Free scale; four arms, any hub	283	1	1.0155
Free scale; four arms, cap-centred hub	256	1	1.0155

Cygnus has fixed R=0.09753151601066437° (0.3901260640426575 quarter-degree units) at astronomical year −2964.4251427554113, or 2965.425143 BCE. The unrestricted runner-up is HIP 17440;16368;15968;13884;16245 in role order, spanning Reticulum, Hydrus and Horologium. Its R=0.21469519640043608° at 2430.125639 BCE gives ratio 2.201290467. Modern regional labels are descriptive only.

The fixed-scale horizon branch contains 17,860 groups with at least one admissible epoch. Cygnus remains first; HIP 56211;52425;47654;50933;52353 is second at 1534.776358 BCE, with R=0.2561224506120477 5° and ratio 2.626048083. In contrast, 13,910 groups satisfy the condition at their unconstrained fixed optimum. Filtering only those optima would omit groups with admissible alternatives, so it is not the implemented horizon comparison. The necessary horizon test does not establish simultaneous night-time observability.

Both four-arm subsets have fixed-scale runner-up HIP 85670;87833;94779;86414;87585, with R=1.2596245287598156° at 1833.144791 CE and ratio 12.915051260. These subsets are nested in the complete nominal census and do not supply independent confirmations.

The free-scale Cygnus optimum is E=0.006490264894093756 (0.6490264894%) at 2985.482488 BCE. Cygnus ranks 68th among all 19,939 groups and first in both four-arm subsets, whose runner-up is centred on HIP 109268 with ratio 1.015506711. The free and fixed Cygnus optima differ by 20.057345 years and both fall in 3000–2920 BCE. Epoch compatibility under these two objectives does not imply scale-independent identification, an uncertainty interval or independent archaeological dating.

The 1-year and 0.5-year searches recover all stated ranks, denominators and leading error ratios. Across all groups, the largest fixed-scale score difference is 1.7582×10^{-8} degree, also the maximum for horizon reoptimization; the largest E difference is 6.7315×10^{-12}. The score tables retain every candidate. Numerical grid agreement is not a proof excluding unsampled continuous-time extrema, and reproduction digits do not represent archaeological or astrometric accuracy.

This complete census has been executed for nominal Hipparcos/J2000 only. The four catalogue/geometry panels and six kinematic variants in sections 2–3 test the earlier cap-centred four-arm ratio family. Their robustness must not be attributed to the full fixed-scale ranking. Alternative target orders and geometric-axis controls in sections 4–7 also retain their own stated universes.

The role rule is explicitly documented in section 2.9 (Nested references and joint persistence) of the separate stellar manuscript identified as related astronomy manuscript; section 2.10 uses the resulting trio and pair. This source verification supports attribution of the algorithm. It does not make the present retrospective field census a preregistered or blinded archaeological test.

S8.10 Calibration by the stellar covering radius

This additional model was formulated after the complete fixed-scale and free-scale rankings were known. The material map supplies W=(28,72,16), r=16 and D=4. We test τ=W/(Dr)=(7/16,18/16,4/16) against equatorial interval fractions $\Delta\alpha_i/\rho$. The radius is $\rho=\max_j \arccos(u_h \cdot u_j)$, centred on the already selected hub. It differs from the minimum enclosing circle with unrestricted centre. No rounding-to-16 gate or preregistration claim is used.

Minimize $E\rho=\sqrt{\{\Sigma_i[\Delta\alpha_i/\rho-\tau_i]^2/3\}}$. Reference-radius searches hold ρ at the geometry epoch; dynamic-radius searches recompute it at each evaluated epoch. For the complete nominal Hipparcos panel, all 19,939 groups and roles remain those of J2000. Both branches span astronomical years −8000 to +2000 on 1-year and 0.5-year grids with bracket refinement and endpoints. Scores are dimensionless fractions of the radius. Using degrees or radians makes no difference; the radius correspondence and factor D remain substantive hypotheses.

Table S8.9. Complete nominal radius-calibrated results and subsets. Main Table 3 summarizes the complete-census rows; this table additionally reports both four-arm subsets.

Radius convention	Candidate family	Groups	Cygnus rank	Error ratio
Reference radius	Complete census	19,939	1	1.316
Dynamic radius	Complete census	19,939	2	—
Reference radius	Four-arm subsets	283 / 256	1 / 1	7.940
Dynamic radius	Four-arm subsets	283 / 256	1 / 1	5.193
Dynamic radius	Necessary horizon	Not counted	1	Not computed

The reference-radius Cygnus score is 0.0066256880851 at 2989.281229 BCE, with ρ=16.238753012°. Its unrestricted runner-up is HIP 60718;62434;66657;61084;61932, at 1281.893 CE, with score 0.008716626429 and ratio 1.315580558. The dynamic Cygnus score is 0.0061549258189 at 2987.991533 BCE; the radius there is 16.22513555°. Its rank is 2 because HIP 37504;34481;29353;35228;39794 reaches score 0.006022884433 near 5742.586679 BCE. Calendar dates are model outputs; printed precision is for reproduction.

The dynamic winner has no admissible epoch under the existing necessary horizon condition at latitude 51.18° N. Each of its five stars has strictly negative maximum upper culmination throughout the search: −15.767450°, −18.896311°, −25.950216°, −19.265389° and −14.448384°, in role order. Both grids and refined extrema agree. Cygnus is admissible at its unrestricted minimum; its five upper culminations are 75.069°, 72.780°, 67.875°, 80.654° and 64.772°. Since imposing a constraint cannot reduce another candidate's minimized score, excluding every unrestricted candidate with error below Cygnus establishes local first place. There is exactly one such candidate. No total feasible-group count or constrained runner-up ratio is inferred; obtaining those would require every group's constrained reoptimization.

A second score implementation uses the physical terrestrial pole n and the absolute atan2 expression given in S8.4. It checks all 19,939 fitted configurations for each radius branch. Maximum score discrepancies are below 5×10^{-12}. Common orthogonal rotations change scores by less than 1.1×10^{-13}, and conversion between degrees and radians changes interval/radius ratios by less than 5×10^{-16}. Across all complete-census candidates, the two-grid maximum score differences are 1.054×10^{-9} (reference) and 2.245×10^{-12} (dynamic), with identical candidate ordering. This independently verifies the score formula, not the shared astrometric engine or continuous-time global optimality.

Catalogue and state sensitivity within the four-arm family

For the four nominal catalogue/geometry panels and six targeted catalogues already archived in 03_Fields, every retained cap-centred four-arm field is refitted under both radius objectives and horizon constraints.

The catalogue identifiers and positions recheck the hub, strict four-arm cycle inequality, geometric role assignment and five-brightest membership at the generating interval midpoint. These tests reuse the archived candidate lists rather than claiming a new complete all-field enumeration. Reference radii use the corresponding geometry epoch, J2000 or 3000 BCE. Targeted catalogues replace only the five Cygnus states in the HYG background; they are shared-background sensitivities, not six independent all-sky surveys.

Table S8.10. Radius-calibrated four-arm sensitivity. Rank columns show unrestricted/local Cygnus ranks. Error ratios are local runner-up/Cygnus; unrestricted ratios and all epochs are archived. No complete 19,939-group sensitivity is claimed here.

Catalogue or state panel	n	Reference rank	Reference ratio	Dynamic rank	Dynamic ratio
Hipparcos J2000	256	1 / 1	7.940	1 / 1	5.193
Hipparcos 3000 BCE	267	1 / 1	11.898	1 / 1	9.461
HYG J2000	255	1 / 1	8.013	1 / 1	5.221
HYG 3000 BCE	261	1 / 1	11.857	1 / 1	9.497
S6 HYG states	255	1 / 1	8.013	1 / 1	5.221
Hip2 PM	255	1 / 1	7.998	1 / 1	5.227
Hip2 RV	255	1 / 1	7.998	1 / 1	5.227
Hip2 HGCA PM	255	1 / 1	8.030	1 / 1	5.252
Albireo A systemic	255	1 / 1	8.294	1 / 1	5.036
Deneb 802 pc	255	1 / 1	8.294	1 / 1	5.036

All four nominal and six targeted panels retain unrestricted and local first place in both branches. In the six targeted scenarios, reference-radius optima span 2987.138–2990.655 BCE and dynamic-radius optima span 2987.081–2989.306 BCE. The smallest local error ratios are 7.9983 and 5.0357, respectively. These ranges describe sensitivity to the specified states and do not measure archaeological dating uncertainty. Both search grids reproduce the ranks and leading ratios; verification files report maximum score differences across every candidate. The slight difference between the homogeneous HYG row and the S6 HYG-state row reflects their separately archived input precision.

Interpretation and limits

The radius supplies a geometric calibration rather than a freely fitted common scale. Thus Eρ can preserve selectivity that E loses in the complete family, while avoiding a fixed degree-per-count equivalence. It adds a chosen relation between spatial extent and temporal intervals; unit cancellation alone does not derive or historically validate that relation. The count map, factor D, five-member field rule, hub and role choices remain. The dynamic complete-census second place and the use of a local necessary horizon condition must remain visible. The four-arm sensitivity cannot be transferred to unrestricted all-field rankings.

Additional geometric diagnostics are retained in 05_RadiusCalibration/other_geometry_diagnostics.json. Among the 256 nominal cap-centred four-arm fields, Cygnus is second in absolute radius-interval width, 32nd in relative width and 12th in tree margin. These are distinct retrospective comparisons and do not establish scale-independent exceptional persistence. None of the radius analyses supplies an independent archaeological observation, a historical probability or evidence that the builders used this calibration.

S8.11 Common-epoch dominance across calibrated objectives

The existing complete-census minima permit a stronger comparison than separately optimized ranks. We evaluate Cygnus at a common epoch and compare each of its objective values with the best unrestricted value of that objective attained by any other field over the original astronomical-year window −8000 to +2000. These rival minima are lower bounds for a competitor evaluated at any common epoch. The audit reuses the archived full-census score tables and recomputes the Cygnus trajectory; it does not claim a new optimization of all rival fields.

Proposition and proof

Let $f_{jk}(t)$ denote objective k for field j, and let b_k be a lower bound on $f_{jk}(t)$ for every rival j and every admissible epoch t. Suppose one Cygnus epoch t_0 satisfies $fC_k(t_0)<b_k$ for every k. Then every nonzero nonnegative weighted sum of these objectives, under arbitrary positive objective normalizations, is strictly smaller for Cygnus at t_0 than for any rival at any admissible epoch. Indeed, multiply each component inequality by its nonnegative weight and positive normalization and sum; at least one coefficient is positive, preserving a strict inequality. Reoptimizing Cygnus can only improve its aggregate score. A strictly increasing aggregate likewise preserves this componentwise dominance. The result concerns weights between the specified objectives, not arbitrary weights on their internal channels.

Complete census and visibility scope

For the fixed angular RMS and the reference-radius RMS, the rival lower bounds are 0.214695196400458° and 0.00871662642854222, respectively. Every Cygnus epoch strictly between 3051.242848 and 2927.266992 BCE improves both bounds. This two-objective statement uses all 19,939 nominal fields without a four-arm or horizon filter. At 2985 BCE the Cygnus scores are 0.101754249492684° and 0.00663722490080135. Thus the assertion compares a common Cygnus epoch against each rival's best possible error in each objective, rather than combining separately chosen Cygnus epochs.

The dynamic-radius field with HIP roles 37504;34481;29353;35228;39794 is permanently invisible under the common necessary horizon rule, as established in S8.10. After removing only that field, the smallest remaining rival unrestricted minimum is 0.00869340078988813. Cygnus improves this bound throughout the same common interval and has score 0.00616100456104537 at 2985 BCE. Its smallest upper culmination over the common interval is 64.726353°. Restricting rival epochs to local feasibility cannot lower any unrestricted minimum. The three-objective dominance statement therefore holds for the common necessary-horizon family, without supplying a new feasible-field count or an exact constrained runner-up margin.

Table S8.11. Common-epoch scores at 2985 BCE and conservative rival lower bounds. The dynamic-radius row uses the necessary-horizon argument above. Values in different rows have different normalizations and are not directly compared.

Objective	Cygnus at 2985 BCE	Rival lower bound
Fixed RMS degrees	0.1017542495	0.2146951964
Reference-radius RMS	0.0066372249	0.0087166264
Dynamic-radius RMS	0.0061610046	0.0086934008

Four-arm comparison and limits

Within the separate 283-field any-member-hub four-arm family, all four objectives, including free-ratio E, share a smaller dominance interval: 2989.279276–2981.680848 BCE. This does not extend the free-ratio statement to the complete family, where Cygnus remains rank 68. Common-epoch dominance does not establish invariance to alternative field generators, count maps, target permutations or arbitrary angular calibrations. A separate fixed-Cygnus-epoch scale-ray diagnostic conservatively retains first place for $0.984952247<s<1.014416558$ when the target is s(7°,18°,4°); it does not identify the full reoptimized winning interval.

The common interval was located independently using the archived 1-year and 0.5-year rival minima, with refined Cygnus threshold crossings. Bounds agree to less than 10^{-6} year; a coordinate-free pole-vector expression agrees with the example scores to 1.23×10^{-14}. The algebraic implication is exact given its numerical premises; the extrema retain the grid-plus-refinement search scope rather than interval-certified global minimization. The interval is a dominance region, not archaeological dating uncertainty, and the objectives share inputs. The standalone Common_Epoch_Dominance_Code_v1_42 archive contains the complete reused score tables, new scripts, outputs and verification record.

Complete angular patterns and unit independent count recovery

Supplementary Material S10

Operational definitions are given in main Methods. This section reports the associated results and derivations; executable instructions and the complete historical records are in Supplementary Data 1.

Lucas Giovani Ribeiro and Marcos André Simonssini
Supplementary Information | Stonehenge v1.47 | 30 October 2026

This appendix develops the fourth relative right-ascension coordinate, its count inverse and the controls needed to interpret its selectivity. It preserves the fixed- and free-scale results, tests freeing or selecting the midpoint, and compares a family generated from the material lengths. These extensions use the same stellar fields as S8; they do not alter the original three-interval census.

S10.1 The missing relative coordinate

The original three channels connect a principal trio and a separate pair. Their signed difference map has rank three. Five right ascensions, after removing one common origin, have four relative degrees of freedom; the three channels therefore leave the pair free to move relative to the trio. Let the hub be zero, the first endpoint have positive offset s_1, the opposite endpoint have offset $-s_2$, and the remaining pair have midpoint b and width s_3. Their four relative positions are $(s_1,-s_2,b-s_3/2,b+s_3/2)$. Here b is the midpoint in wrapped right ascension on the local branch, not the right ascension of a spherical geodesic midpoint.

Inspection of the archived Cygnus coordinates suggested the added relation $b=-s_1/D$. For D=4 and W=(d,3q,r)=(28,72,16), it produces the following register:

$$T = (d,\ -3q,\ -d/D - r/2,\ -d/D + r/2) = (28,\ -72,\ -15,\ 1).$$

The hub has coordinate zero. For Cygnus, the remaining positions are Deneb, Albireo, Fawaris and Aljanah in this order. The original interval word does not require this displacement relation. It was introduced after the earlier Cygnus results were available.

A construction in the existing frame (x,y,z)=(10,24,26) produces the same register using bisections and differences:

$$T = (2z - y,\ -3y,\ x/2 + y/4 - z,\ y/4 - x/2).$$

Its pair midpoint is y/4−z/2=−7 and width is z−x=16. This gives a geometric realization of the new relation; assigning these constructions to stellar positions remains an additional modelling choice. Four relative positions determine all ten pairwise right-ascension differences, but those ten differences are not independent confirmations. Declinations and full archaeological positions are not reconstructed by this one-dimensional register.

S10.2 Full census with fixed angular scale

Cygnus ranks first at R_4=0.081192402° near 2949.136 BCE. The runner-up, with ordered HIP roles 13847;12413;9459;11407;12486, has R_4=0.660640418° near 2672.252 BCE: an error ratio of 8.1367. The largest annual-versus-half-year score difference is 4.37×10^{-11} degrees.

A matched ablation allows the pair midpoint to be free at every epoch, retaining the fixed principal targets and pair width. Its squared loss is $[(z_1-7)^2+(z_2+18)^2+(w-4)^2/2]/4$, where w is the minor wrapped width of the remaining pair. Cygnus remains first near 2949.038 BCE, but the runner-up ratio is 1.9597. This isolates the added midpoint restriction within that loss family. It is not a direct ablation of the earlier three-channel R objective, which uses different residual weights.

Table S10.1. Complete-pattern comparisons. All rows use 19,939 fields except the final 283-field subset. Ratios apply only to the stated model and family. The 66-description rows allow each field its own best relation, scale and epoch.

Model	Cygnus score	Epoch BCE	Rank	Error ratio
Fixed four positions	0.081192402°	2949.136	1	8.1367
Fixed with free midpoint	0.080757204°	2949.038	1	1.9597
Free-scale four positions	0.005504994	2975.932	1	2.2234
Free scale and free midpoint	0.005246934	2976.701	119	—
Best of 66 descriptions	0.005504994	2975.932	16	—
Best of 66, four-arm subset	0.005504994	2975.932	1 / 283	Not computed

S10.3 Scale free comparison of the complete pattern

The complete census gives Cygnus first place at L=0.005504994, or a 0.550499% normalized residual, near 2975.932 BCE. The runner-up has L=0.012239857 near 1360.879 BCE and ordered HIP roles 92420;93194;95372;92791;93279. The error ratio is 2.2234. Cygnus also ranks first within the 283 any-member four-arm fields, although that filter is unnecessary for the reported complete-census first place.

The fitted conversion is 0.251667709° per register unit and the angular RMS after fitting it is 0.054518834°. Thus a value close to one quarter degree emerges from this fit; it is not fixed in this objective. The largest cross-grid score difference over all 19,939 candidates is 1.53×10^{-9}. The epoch lies about eleven years from the original fixed-scale optimum and ten years from the original three-interval ratio optimum. These differences compare model outputs, not archaeological dating errors.

The three-interval free-scale result remains rank 68. Completing the pattern adds a relative coordinate and changes the residual definition. The 2.2234 ratio is conditional on the specified midpoint relation; the 8.1367 fixed-pattern margin belongs to a different objective. No full alternative-catalogue recensus, horizon-constrained margin or common-epoch dominance theorem is asserted for L.

Matched midpoint ablation and relation-choice control

Let T_0=(28,−72,−8,8) and e=(0,0,1,1). Freeing the pair midpoint while retaining the original normalization gives $L_0 = min_{a \geq 0, \beta} \| z - aT_0 - \beta e \| / \| z \|$. Because T_0 and e are orthogonal, the minimizing displacement is $\beta=(z_3+z_4)/2$, and $a=\max(0, z \cdot T_0/6096)$. This is a nested relaxation of the specified-midpoint model. Its complete two-grid census ranks Cygnus 119th at L_0=0.005246934 near 2976.701 BCE. The first place under the original L therefore depends on the midpoint relation extracted from Cygnus.

Cygnus retains h=−28/4 and its original score and optimum, but ranks 16th among all 19,939 fields. Its rank is first within the already defined 283-field four-arm subset. The overall winner has HIP roles 8903;8832;8387;7981;9110, h=−16/12, L=0.001057521 and an optimum near 7621.826 BCE. The 15 fields ahead of Cygnus are outside the four-arm subset. The complete-family result remains the primary control; the subgroup result is reported separately and does not restore unrestricted first place.

The earlier rank 228 refers only to midpoint-equality mismatch over the 66 descriptions at the common 2965.425 BCE epoch. It is not the complete-pattern, full-epoch comparison above. The new family search accounts for this finite relation choice while retaining the original word, field generator, role rule, coordinate frame and family bounds. It is a retrospective sensitivity analysis, not a global false-positive probability.

S10.4 A conditional inverse independent of angular units

Assume $b=-s_1/D$ and the previously stated closure $r=D^2$. Let K convert the measured angular intervals into register units. Then:

$$D = -s_1/b, \qquad K = D^2/s_3.$$

$$A = D + K(s_1+s_2/3),$$

$$B = K[(s_1-s_3)/2+s_2/3], \qquad C = D + K(s_1-s_3)/2.$$

To derive the inverse, set $d=Ks_1$, $q=Ks_2/3$ and $r=Ks_3=D^2$ in the original compiler. Its three identities give $C=D+(d-r)/2$, $B=q+C-D$ and $A=B+C+r$, yielding the expressions above. Under an angular-unit conversion $s_i \to cs_i$ and $b \to cb$ with $c>0$, D is unchanged and $K \to K/c$. All four recovered counts are therefore unchanged. Neither integer rounding nor the other two closure equations is needed for this algebra.

At the new nominal free-scale epoch, the offsets in degrees are (6.951275495,−18.161460806,−3.752874906,0.275775297). They give D=3.998318297 and K=3.968214762 units per degree. The continuous inventory and its nearest-integer interpretation are shown below. K comes from the quadratic closure; it is not constrained to equal the inverse fitted scale 1/a in imperfect data.

Table S10.2. Unit-independent inverse at three nominal epochs. Rounding is nearest integer; these continuous values are not an exact integer identity.

Epoch BCE	A	B	C	D	Rounded inventory
2965.425	55.21075	29.54173	9.69781	3.99640	55,30,10,4
2985.482	55.96830	30.07926	9.88853	4.00006	56,30,10,4
2975.932	55.60533	29.82166	9.79712	3.99832	56,30,10,4

The six archived stellar-state alternatives also round to (56,30,10,4) at the new nominal epoch. Their A values span 55.56846–55.73667. At 2965.425 BCE all six alternatives, as well as the nominal state, instead round A to 55. The original ratio epoch rounds all seven states to the target inventory. These evaluations hold the three nominal epochs fixed; they do not reoptimize every state or recensus its rivals.

The astronomical target used to fit the epoch already came from the known inventory, and the displacement relation was recognized retrospectively. These inverse calculations therefore establish conditional consistency and its temporal limits, not recovery of previously unknown archaeological counts. Imposing all three original closures would independently force (56,30,10,4); only $r=D^2$ is used in this angular inverse.

S10.5 Material and procedure diagnostics

In the ideal frame, the +1 endpoint is y/4−x/2: the difference between the model Z-circle and sarsen-circle radii, 6u−5u. The rounded observed diameters, 39 m and 33 m, instead give a radial gap of 3.0 m. Relative to the exterior scale 3.3314 m, this is 0.9005u, about 10% below the ideal. The algebraic interpretation is therefore not a new precise metric confirmation, and features from different phases cannot be treated as one contemporary construction solely from this relation.

A separate exploratory test uses the 56 manually digitized Cleal Aubrey symbols and four heterogeneous Station proxies already available in the archive. Correlated tangential residuals are compatible with several procedures. The small-sample Akaike criteria are 35.852 for a closed-walk covariance, 36.023 for the 7|21|7|21 sector model and 36.523 for a generic cyclic AR(1) covariance. Their near tie does not identify a unique setting-out operation. The Station-anchored sector phase ranks 12th among 28 integer phase alternatives. After removal of a global rotation, the closed-walk covariance cannot identify a starting point.

An exact 5:12:13 rectangle fits the four Station proxies at 0.415 m RMS, compared with 0.481 m for the regular-56 seven-step rectangle, a 13.8% reduction. Under equal orientation freedom, the two ideal rectangles differ by about 0.0904 m per vertex at the adopted diameter. Digitized drawing proxies lack the positional uncertainty model needed to turn this difference into a decisive archaeological discrimination. These diagnostics use existing drawing information; no unexcavated-hole holdout or new georeferenced survey is claimed.

S10.6 Information order and reproducibility

The original word, fixed-scale epoch and later field comparisons preceded this extension. The fourth-coordinate audit first showed that the original intervals leave a displacement unspecified and that centring the remaining pair at the hub fails. The relation $b \approx -s_1/4$ was then recognized from the Cygnus outputs. A limited 66-description comparison of signed channels and divisors was recorded before the complete four-position fixed census. Its conditional ranks, including adverse ones, are retained in the code outputs and are not global false-positive probabilities. The free-scale four-position census and unit-independent inverse followed the fixed-pattern result.

The supplied PROTOCOL.json files record choices for their respective executions. They were not public preregistrations made before observing the relevant pattern. The archaeological evidence is unchanged. Historical attribution requires an unused observation that discriminates this proposed procedure from competing complete models; the present extension supplies explicit predictions and a computational comparison, not a probability of intention.

S10_Code contains 01_Procedures, 02_Fourth_Link, 03_Unit_Free and the subsequent 04_Midpoint_Controls. Their input and result files preserve the delivered diagnostic archives. Each directory retains its original reproduction commands and dependencies. The two complete pattern censuses used annual and half-year grids with minimum refinement. The unit-free verifier independently recomputes the top ten scores from projected vectors and least squares, checks 5,000 synthetic inversions, and verifies invariance to unit conversions. The maximum synthetic inverse error is 3.70×10^{-13}, and the maximum loss change under unit conversion is 1.12×10^{-15}. These are numerical checks using the archived precession engine.

The earlier fixed-pattern verifier checked 1,990 admissible synthetic inventories and independently recomputed and refined the first ten candidates of both its fixed and free-midpoint models. Six archived state alternatives supplement the nominal Cygnus calculation; they are not a rival recensus. The construction-error module has a clean-run reproduction record. The v1.43 integration checked preserved bytes and reran the then-available numerical verifiers. No new complete execution of S1–S8 or new astrometric catalogue comparison is claimed. Cache arrays can be regenerated and are excluded from the transport archive.

Revision v1.44 adds the matched ablation and finite-family controls after the v1.43 results were known. The 66-description family was already archived; its joint complete-pattern execution is new. An independent projected-vector and least-squares verifier checks all 19,939 ablation optimum scores and all 18,480 eligible template optimum scores, with local refits of leading cases. Ten evaluations at zero-offset orientation boundaries are checked through their one-sided limits; none affects the leading ranks. Earlier outputs remain unchanged.

S10.7 A census of material midpoint rules

Only $h=-7$ retains Cygnus first: 1/47 (2.13%) in the primary construction family, 1/73 with inventory lengths, 1/129 with register lengths and 1/139 in their union. The same h reproduces the original L=0.005504994 result near 2976 BCE and its 2.2234 error ratio. Thus the material lengths can express the successful relation, but this library of material operations does not select it uniquely or yield first place across a broad fraction of rules. These fractions describe this finite family; they are not probabilities of historical intention.

This family was specified after the prior Cygnus outcomes were known, before its own census. S10_Material_Rules contains its protocol, code, inputs, results and verification. Its README explains regeneration of the omitted intermediate score array before running the full verifier. Earlier results and source files are preserved.

Woodhenge counts and chronological comparison

Supplementary Material S11

Lucas Giovani Ribeiro and Marcos André Simonssini

S11.1 Archaeological inputs and information order

The numbered concentric rings A–F in the published Woodhenge plan [33, Fig. 2, printed p. 4] supply the outer-to-inner sequence (60,32,16,18,18,12). The analysis concerns those numbered ring positions. Their total is 156, whereas the report describes 168 excavated postholes overall. The present transcription does not assign the difference to repairs, duplicates or external structures. No additional positions have been inserted into the six-ring vector.

Table S11.1. Ring inputs and their roles in the exploratory extraction.

Ring	Variable	Count	Occurrence in the extraction
A	n_1	60	$w_1=n_1-n_2$; $w_2=n_1+n_6$
B	n_2	32	$w_1=n_1-n_2$; $w_3=n_2-n_6$
C	n_3	16	Closure $n_2=2n_3$
D	n_4	18	Closure $n_1=2(n_4+n_6)$
E	n_5	18	Closure $n_4=n_5$
F	n_6	12	$w_2=n_1+n_6$; $w_3=n_2-n_6$

Marshall et al. model a unitary construction episode by combining the date distributions for rings A, B and C [33, pp. 14–15, Fig. 5]. Its 95% interval, 2635–2575 cal BCE, is the benchmark here. The higher-density intervals reported separately are 2635–2610 cal BCE (54%) and 2595–2580 cal BCE (14%). Inclusion in the 95% interval is not a comparison with the full posterior density, nor evidence that the astronomical minimum coincides with its mode. Rings D–F are not separately dated by that combination.

The earlier analysis selected each target entry as the closest value among positive pairwise sums and absolute differences of ring counts at the already-known date of 2600 BCE. This produced (28,72,20), subsequently represented as (n_1-n_2,n_1+n_6,n_2-n_6). The closures, ring-to-operation association and integer decoder were also formulated with Woodhenge known. The present census exhausts the declared arithmetic family after this selection. S11_Woodhenge/denominator_audit/earlier_selection_record.json preserves the initial selection record; PROTOCOL.json specifies the subsequent audit. Neither is a public prospective registration.

S11.2 Complete arithmetic family and temporal search

For each pair of distinct ring slots i<j, form n_i+n_j and $|n_i-n_j|$ and retain positive values. Collapsing numerical duplicates gives the alphabet {2,4,6,14,16,20,28,30,34,36,42,44,48,50,72,76,78,92}. Its ordered Cartesian cube contains $18^3=5{,}832$ targets; values and ring pairs may be reused across channels. Distinguishing arithmetic descriptions instead gives 29 positive expressions and $29^3=24{,}389$ ordered descriptions. The target 28 can arise from 60−32 or 16+12, so (28,72,20) has multiplicity two.

Each target W is divided by four and compared with the three Cygnus intervals using the RMS objective and archived Hipparcos propagation/precession model in main section 2.3. Cygnus and stellar roles remain fixed. For every target, astronomical years −8000 to +2000 are scanned on 1-year and 0.5-year grids. All detected interior minima are refined by bounded scalar minimization, both endpoints are retained, and the lowest score defines the numerical global optimum. The archaeological interval does not constrain this primary optimization. A secondary calculation allows every word its best fit inside that interval.

Table S11.2. Primary census and chronological comparisons. Both search grids agree on every count below. Numerical rank is by RMS across all epochs; a candidate family is not an equiprobable null distribution.

Comparison	Result
Distinct ordered numerical targets	5,832
Global minimum within 2635–2575 BCE	33
Global minimum in that interval and RMS <0.2°	1
Global minimum in that interval and RMS ≤0.169091271°	1
Rank of (28,72,20) without chronological restriction	6
Targets with RMS <0.2° at any epoch	7
Next best target optimized inside the archaeological interval	(30,72,20); 0.416338°
Its error divided by the candidate error	2.4622

With expression multiplicity retained, 141 descriptions have their global minima in the interval, and two also reach the candidate error. These two descriptions represent the same numerical target. The numerical and expression denominators are descriptive counts, not p-values. The full-window census does not undo the date-informed initial selection.

S11.2.1 Random inventories and date-informed selection

The within-Woodhenge census counts alternatives generated from one observed inventory. We additionally replace that inventory with six independent uniform integers from 10 through 60, with replacement, and regenerate its positive pairwise sum/difference alphabet and ordered target family. A second distribution samples only even integers in the same range, reflecting the observed all-even inventory. Each distribution supplies 1,000 inventories. NumPy default_rng (PCG64), seed 20261030, generates the general uniform block first and then the even block. Cygnus, stellar roles, quarter-degree calibration, epoch range and archaeological interval remain fixed.

The primary event is the existence of a family target whose full-window global minimum lies in 2635–2575 BCE and whose RMS is no greater than the observed 0.1690912706°, using a numerical tolerance of 10^{-10} degree. Thus each random inventory receives the same freedom to choose its best qualifying word. A separate replay selects each coordinate nearest to the known 2600 BCE sky, as in the original exploration, before optimizing that single word globally. The all-epoch diagnostic asks whether any family word reaches RMS below 0.2° without a chronological condition.

Table S11.2a. Random-inventory reference frequencies. The first two result columns require a global optimum inside the archaeological interval and RMS no greater than observed. The last column drops the chronological condition and uses the 0.2° threshold.

Count distribution	Any qualifying word	Replay at 2600 BCE	Any epoch below 0.2°
Uniform integers 10–60	33/1,000 (3.3%)	24/1,000 (2.4%)	917/1,000 (91.7%)
Even integers 10–60	105/1,000 (10.5%)	105/1,000 (10.5%)	882/1,000 (88.2%)

The primary frequencies have 95% Wilson Monte Carlo intervals of 2.36–4.60% and 8.75–12.55%, respectively. These quantify finite-simulation uncertainty under each count distribution. Among the first 300 general-uniform inventories, 12 meet the primary event and 280 pass the all-epoch diagnostic. Chronological agreement adds discrimination beyond a small angular residual alone; the difference between distributions shows sensitivity to count parity. These artificial inventories are conditional reference models, not an empirical distribution of archaeological monuments or a correction for all retrospective choices.

For integer targets in 1–120, numerical screening around the astronomical curve and full-window refinement identify 655 targets below 0.2° on both the 1-year and 0.5-year grids. Only (27,72,20), at 2594.019 BCE with RMS 0.131477°, and (28,72,20) meet the joint primary criterion. Membership therefore reduces to the alphabet containing 72 and 20, together with 27 or 28; the odd alternative is unavailable to all-even inventories. The two grids give identical qualifying sets and reproduce Woodhenge's seven low-error words and rank six. A separate Boolean-membership implementation verifies all 2,000 inventories, selection replays and forward objectives. This reuses the archived astronomical model; grid agreement is a numerical check rather than a continuous-time interval certificate.

The random comparison was specified after the exploratory result and an external report of the proposed control were known. Its protocol, complete inventory table, qualifying targets and verifier are archived in S11_Woodhenge/random_inventory_reference. The calculation adds a reference distribution to the existing retrospective census; it does not change the selection history in S11.1.

S11.3 Chronological concordance and alternatives

The target (28,72,20) reaches RMS 0.1690912706° near 2608.908 BCE, within the unitary construction interval. The digits locate a model minimum; they do not express archaeological dating precision. The next word among the 33 with global minima in that interval is (16,76,20), RMS 1.763112°. The broader interval-constrained comparison instead gives (30,72,20), RMS 0.416338°, at 2635 BCE. These two runner-up definitions must not be interchanged.

Table S11.3. The seven targets with global RMS below 0.2°. The Stonehenge target is also an arithmetic member of the Woodhenge family and achieves a smaller error at a different epoch.

Rank	Target	Epoch BCE	RMS degrees	In interval
1	(30, 78, 2)	4439.83	0.047084	No
2	(30, 78, 4)	4266.42	0.077020	No
3	(28, 72, 16)	2965.43	0.097532	No
4	(34, 92, 28)	7283.78	0.130702	No
5	(30, 76, 6)	4021.35	0.136366	No
6	(28, 72, 20)	2608.91	0.169091	Yes
7	(30, 78, 6)	4091.86	0.188941	No

At the Stonehenge optimum, the celestial intervals expressed in quarter degrees are (27.7891,72.6055,16.2134); at the Woodhenge optimum they are (27.2403,71.2289,19.5521). Their changes are (−0.5489,−1.3766,+3.3387) quarter degrees, or (−0.1372°,−0.3441°,+0.8347°). The third channel changes most, corresponding approximately to the target change 16→20. The other two channels are not constant. The new extraction differs from the Stonehenge count map, so the agreement does not establish a single decoder transferred unchanged between monuments.

Temporal response of the two targets

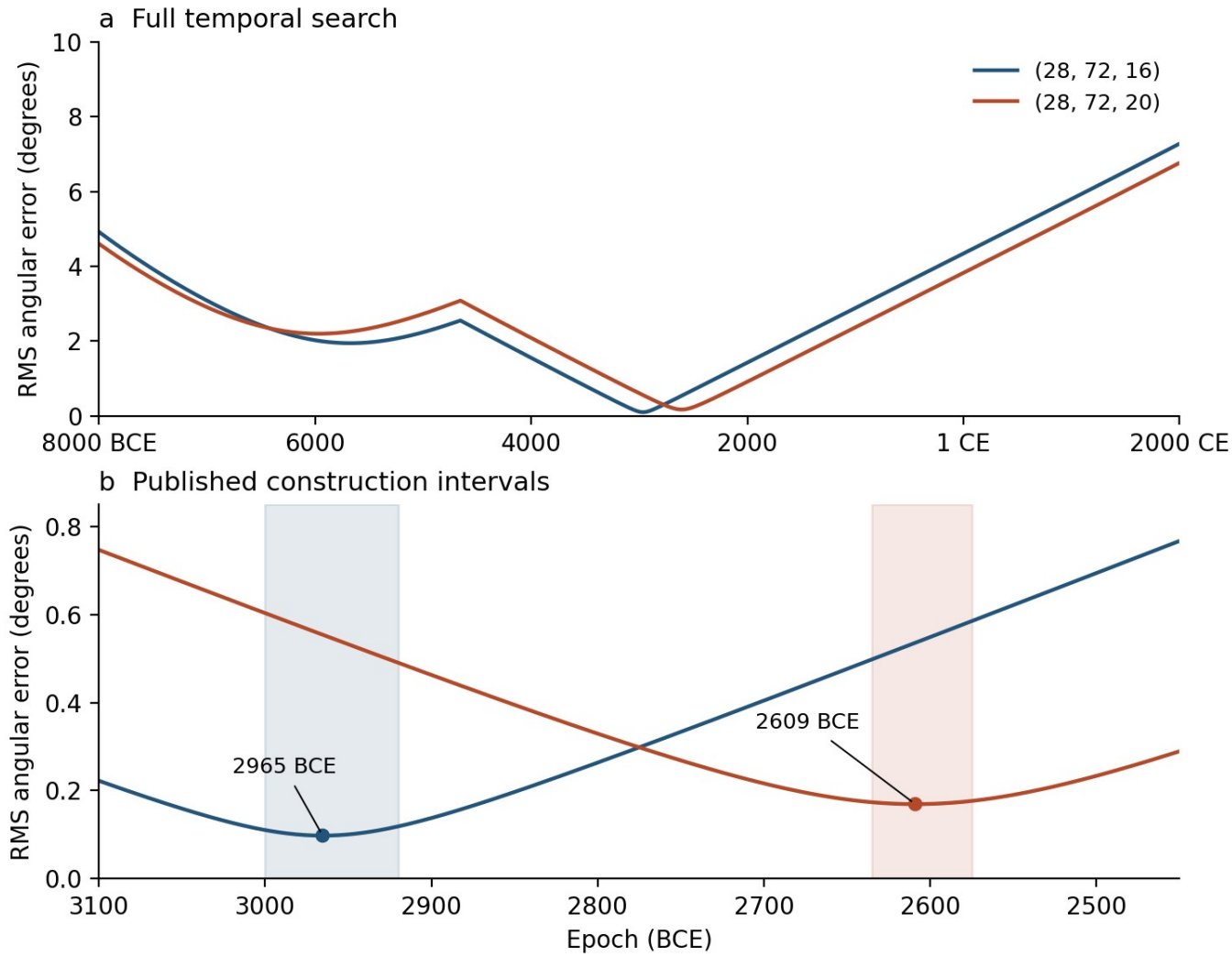


Figure S11.1. The same Cygnus clock compared with two angular targets. (a) RMS curves over the complete search window using the common Hipparcos inputs. (b) The minima near 2965 and 2609 BCE and the initial-enclosure interval for Stonehenge [2] and unitary timber-construction interval for Woodhenge [33]. Shading reproduces published intervals, not confidence bounds from the astronomical model. Woodhenge's target was selected with its approximate chronology known. The curves illustrate the ensuing comparison and do not constitute a prospective dating test.

The substantive result combines target fit with chronological location. Table S11.3 retains the high-quality fits at other epochs. The random-inventory comparison shows why both conditions matter and measures the dependence on the chosen count distribution. Within Woodhenge's declared arithmetic family, (28,72,20) uniquely meets the joint criterion.

S11.4 Material transcription between the inventories

A separate ring association reuses the Stonehenge quantities B=30, r=16 and q=24: (2B,2r,r,B−q/2,B−q/2,q/2)=(60,32,16,18,18,12). It reproduces the complete numbered ring sequence without stars, dates or angular units in the calculation. The ring-to-operation association was chosen with the Woodhenge counts known; reuse of earlier operations does not make the association a prior prediction.

Inverting the association gives $B=n_1/2=30$, $r=n_3=16$ and $q=2n_6=24$. If r is diagonal minus short side, set $z=x+r$ and impose $x^2+q^2=z^2$. Then $x=(q^2-r^2)/(2r)=10$, $z=26$ and the inradius is $D=(x+q-z)/2=4$. Taking C=x and A=B+C+r recovers (A,B,C,D)=(56,30,10,4). The other ring counts check the duplicated expressions 2r and B−q/2. The Pythagorean identity is a condition of this inverse, not an additional independent observation.

Table S11.4. The five previously archived measurement branches under the same association. All give the observed six counts after nearest-integer rounding; the largest discrepancy refers to any one continuous count.

Aubrey or diagonal branch	z metres	Largest count discrepancy
Thom	86.44000	0.178665
Hawkins	86.87000	0.008589
Lawson	87.00000	0.053910
MacKie prose	85.83168	0.433018
Euclidean	86.79348	0.031685

A dimensionless branch retains B=30 and C=10 and uses the side ratio t=y/x: q=Ct and $r=C(\sqrt{(1+t^2)}-1)$. The observed ratio t=80.095/33.435=2.395543592 produces the same rounded sequence throughout $2.372893803<t<2.427060980$. Among the 16 primitive frames already used in main section 3.1, only 5:12:13 gives all six rounded counts under this fixed new association. This comparison tests that association; it does not enumerate all possible assignments of rings to operations.

The recovered Stonehenge inventory returns (28,72,16) under the original count map. The direct Woodhenge extraction returns (28,72,20). These are separate mappings of the same ring inputs, not independent confirmations of a unique date.

S11.5 Conditional recovery and geometric controls

The six counts satisfy $n_2=2n_3$, $n_4=n_5$ and $n_1=2(n_4+n_6)$. With $c=n_3$, $d=n_4$ and $f=n_6$, the integer family is $n=(2(d+f),2c,c,d,d,f)$, and its target is $W=(2(d+f-c),2d+3f,2c-f)$. The linear map has determinant magnitude eight. Integral inversion requires an even w_1 and a total $w_1+w_2+w_3$ divisible by four, together with positivity of all counts and intervals. These conditions follow from the stated closures; no all-even condition is imposed.

At the Woodhenge optimum, joint nearest-admissible-word decoding recovers (28,72,20) and hence all six counts. The runner-up (26,71,19) corresponds to (58,32,16,16,16,13), RMS 0.198720°, a ratio of 1.1752. Direct inversion of the real celestial intervals followed by independent rounding instead gives (59,32,16,17,17,12), which fails a closure. Both outcomes are retained: joint decoding and independent rounding solve different approximation problems.

A finite lattice-neighbour calculation and a full-window 1-year scan give a single recovery interval, with refined switching epochs near 2709.040 and 2557.679 BCE. It contains the archaeological interval. These are decoder boundaries, not dating confidence limits. At the best epoch, the nearest decision boundary lies approximately 0.01541° away in RMS interval space, showing the modest perturbation margin. The construction remains conditional on the retrospectively specified relations, Cygnus and calibration.

A separate preliminary digitization of rings B and C examines whether the 32:16 relation also carries a distinctive shared positional-error pattern. Alternating-ray RMS is approximately 5.28°. Ellipse normalization gives gap correlation 0.763, but competing alignments reach 0.831 and 0.824; removing a smooth second harmonic reduces the assigned correlation to 0.466. These drawing-proxy diagnostics do not establish copied local errors or a setting-out procedure. Pixel coordinates and all comparisons are retained.

Durrington was considered under a privately recorded eligibility protocol after the Woodhenge construction. The inspected sources did not supply a verified complete six-ring count vector from one phase meeting that protocol. No Durrington date was computed; its outcome is indeterminate at input eligibility. This is not a successful external replication or a negative chronological test.

S11.6 Reproduction and verification

Supplementary Data 1 contains S11_Woodhenge with the frozen astronomical inputs, all 5,832 optimized rows from each search grid, refined local minima, expression multiplicities, model definitions and the earlier exploratory record. The published plan and report are cited at their source; the third-party raster is not redistributed. The numerical files contain the ring and proxy transcriptions needed by the calculations. The random_inventory_reference subdirectory adds the 2,000 inventory draws, both count distributions, target lists and selection replay. Its initial reading notes describe the earlier standalone audit; the current inclusion in S11 is documented in README_CURRENT.txt.

From S11_Woodhenge, reproduce the principal audit with:

```
python denominator_audit/audit_words.py
```

```
python denominator_audit/verify_results.py
```

```
python material_bridge/check_material_bridge.py
```

```
python lattice_decoding.py
```

python random_inventory_reference/audit_random_inventories.py

python random_inventory_reference/verify_audit.py

The census uses Python 3.12.14, NumPy 2.3.5 and SciPy 1.17.0. Its verifier checks all 5,832 distinct words, recomputes all 11,664 archived objective values, checks input hashes and reproduces the principal denominators. The maximum objective discrepancy is below 4×10^{-15} degree. The same astronomical implementation is used; this is an integrity and numerical consistency check, not an independent physical-model implementation.

The sole difference in detected local-minimum counts is the target (30,78,76): a shallow minimum lies near astronomical year 1999.642, just before the upper boundary. The 1-year grid retains the boundary and the 0.5-year grid resolves the interior minimum, with RMS about 4.647°. Explicit refinement resolves the discrepancy; it affects neither chronological membership nor the error thresholds. Agreement between grids remains numerical rather than an interval certificate of global minimization.

The result is an enumerated retrospective concordance, with its date-informed selection, complete alternative family and random-inventory comparisons documented together. Material transcription, integer recovery and plan diagnostics analyze the same chosen construction and are not multiplied as independent evidence. Historical attribution requires archaeological support for the extraction and transmission of these operations.